Genetics and Genomics

A transcription network underlies the dual genomic coordination of mitochondrial biogenesis

Reviewed Preprint
v2 • November 27, 2024
Revised by authors

Reviewed Preprint
v1 • May 14, 2024

Fan Zhang, Annie Lee, Anna Freitas, Jake Herb, Zongheng Wang, Snigdha Gupta, Zhe Chen, Hong Xu

National Heart, Lung, and Blood Institute, National Institutes of Health, Bethesda, USA

eLife Assessment

This study's findings substantially advance our understanding of an **important** aspect of mitochondrial metabolism. The data are **compelling** and the study is well executed. The work is relevant to all who are interested in the biogenesis of mitochondria.

https://doi.org/10.7554/eLife.96536.2.sa3

Abstract

Mitochondrial biogenesis requires the expression of genes encoded by both the nuclear and mitochondrial genomes. However, aside from a handful transcriptional factors regulating specific subsets of mitochondrial genes, the overall architecture of the transcriptional control of mitochondrial biogenesis remains to be elucidated. The mechanisms coordinating these two genomes are largely unknown. We performed a targeted RNAi screen in developing eyes with reduced mitochondrial DNA content, anticipating a synergistic disruption of tissue development due to impaired mitochondrial biogenesis and mtDNA deficiency. Among 638 transcription factors annotated in Drosophila genome, 77 were identified as potential regulators of mitochondrial biogenesis. Utilizing published ChIP-seq data of positive hits, we constructed a regulatory network revealing the logic of the transcription regulation of mitochondrial biogenesis. Multiple transcription factors in core layers had extensive connections, collectively governing the expression of nearly all mitochondrial genes, whereas factors sitting on the top layer may respond to cellular cues to modulate mitochondrial biogenesis through the underlying network. CG1603, a core component of the network, was found to be indispensable for the expression of most nuclear mitochondrial genes, including those required for mtDNA maintenance and gene expression, thus coordinating nuclear genome and mtDNA activities in mitochondrial biogenies. Additional genetics analyses validated YL-1, a transcription factor upstream of CG1603 in the network, as a regulator controlling CG1603 expression and mitochondrial biogenesis.

Introduction

Mitochondria respiration, carried out by the electron transport chain complexes (ETC), converts the energy in chemical fuels to the electrochemical potential across the mitochondrial inner membrane ($\Delta\psi_m$) that drives the synthesis of ATP. Deficient ETC not only impairs energy metabolism, but may also disrupt cellular redox balance and various biosynthetic pathways (Shen et al., 2022; Spinelli and Haigis, 2018), and is associated with various human diseases (Gorman et al., 2016). Mitochondria are under dual genetic control. Their own genome, mitochondrial DNA (mtDNA) encodes 13 core subunits of ETC, alongside 2 rRNAs and 22 tRNAs that are required for the translation of these protein-coding genes inside the mitochondrial matrix (Chen et al., 2019).

The majority of more than 1000 mitochondrial proteins including the remaining ETC subunits, factors for mtDNA replication and transcription, and mitochondrial ribosomal proteins are all encoded on the nuclear genome (Hock and Kralli, 2009; Taylor and Turnbull, 2005). The mitochondrial transcription factor A (TFAM) compacts mtDNA into nucleoids and is a key regulator of mtDNA copy number (Alam et al., 2003; Scarpulla, 2008). TFAM, together with other auxiliary factors including mtTFB1 and mtTFB2, promotes the transcription of mtDNA by mitochondrial RNA polymerase (POLRMT) into long polycistronic precursor RNAs, which are further processed into individual RNAs (Chen *et al*., 2019; Falkenberg et al., 2002). POLRMT can also generate short RNA oligos, owning to its exoribonuclease activity, to prime mtDNA replication by polymerase γ (Liu et al., 2022). Nuclear-encoded mitochondrial proteins are synthesized in cytoplasm and imported into mitochondria (Wiedemann and Pfanner, 2017). Hence, mitochondrial biogenesis is influenced by the abundance and activities of mitochondrial translocases as well. The intricate interplay between mitochondrial and nuclear-encoded components demands coordinate activities of these two genomes, to maintain the efficiency and integrity of oxidative phosphorylation system and other critical mitochondrial processes (Hock and Kralli, 2009; Scarpulla, 2008).

Mitochondrial respiration, particularly, the contents and the activity of ETC, is fine tuned to cope with the developmental and tissue-specific metabolic demands (Fernandez-Vizarra et al., 2011). Various transcriptional cascades have emerged as effective and adaptable mechanisms regulating ETC biogenesis. The nuclear respiration factors, NRF1 and NRF2 activate the expression of many nuclear-encoded ETC subunits and genes essential for mtDNA replication and transcription (Scarpulla, 2008). This regulation allows NRFs to indirectly control the expression of mtDNA-encoded genes, and hence coordinate the activities of both genomes in ETC biogenesis. The peroxisome proliferator-activated receptors (PPARs), upon activation by diverse lipid ligands, induce the expression of nuclear genes in fatty acids oxidation pathway (Berger and Moller, 2002). Another family of nuclear receptors, the estrogen-related receptors (ERRs) regulate nuclear genes involved in oxidative phosphorylation, including ETCs and the citric acid (Deblois and Giguere, 2011). Notably, all forementioned transcription factors share a common co-activator, PPARγ coactivator-1α (PGC-1α) that directly stimulates the basal transcriptional machinery (Finck and Kelly, 2007; Hock and Kralli, 2009; Scarpulla et al., 2012). PGC-1α and related coactivators are dynamically regulated in responses to various physiological or environmental cues, to adjust metabolic program and energy metabolism accordingly (Hock and Kralli, 2009; Scarpulla *et al*., 2012). Members of PPARs or ERRs families often show tissue-specific expression and regulate subsets of mitochondrial genes (Deblois and Giguere, 2011; Hock and Kralli, 2009). However, given the large number and diverse evolution origins of mitochondrial genes (Kurland and Andersson, 2000; Rath et al., 2021), the current understanding on transcriptional regulation of mitochondrial biogenies appears incomplete. Additionally, mechanisms coordinating nuclear genome and mtDNA activities in ETC biogenesis remain unclear.

Recently, the modERN (model organism Encyclopedia of Regulatory Networks) project generated genome-wide binding profiles of a large set of transcription factors in *C. elegans* and *Drosophila melanogaster* (Kudron et al., 2018). The global mapping of transcription factor (TF)-DNA interactions could potentially be applied to identify the transcriptional network governing mitochondrial biogenesis. However, the DNA binding profiles of TFs have their limitations in understanding the true biological functions of TFs in gene regulation (Jiang and Mortazavi, 2018). Gene expression is, in most cases, subject to the combined influences of multiple TFs. Additionally, an individual TF may have either activating or repressive roles based on the local chromatin environment (Jiang and Mortazavi, 2018). Furthermore, despite the substantial progress in bioinformatics analyses, the interpretation of genome-wide omics data still has its limitations due to a lack of robust statistical algorithms, variations in biological contexts, and intrinsic experimental variations (Angelini and Costa, 2014; Zhou et al., 2016). The integration of the DNA binding profiles with functional genetic and genomic studies is ideal to study gene expression regulations (Jiang and Mortazavi, 2018; Park, 2009).

The *Drosophila* eye is an excellent model for genetic analyses due to its ease of assessment and minimal impact on other physiological processes in the presence of developmental abnormalities. The cell proliferation and differentiation during eye development require robust mitochondrial respiration, and adult eyes are severely disrupted by mutations affecting nuclear ETC subunits or mitochondrial translation apparatus (Liao et al., 2006; Owusu-Ansah et al., 2008). We previously developed a genetic scheme to generate mtDNA deficiency by expressing a mitochondrially targeted restriction enzyme (Chen et al., 2015; Xu et al., 2008). In this study, we performed a RNAi screen, targeting 638 transcription factors annotated in the *Drosophila* genome, in the presence of mtDNA deficiency in developing eyes. We recovered 77 TFs, RNAi against which had synergistic effects with the mtDNA deficiency in causing the small-eye phenotype. We further followed up on CG1603, one of the strongest hits from the initial modifier screen and revealed that it was essential for coordinating nuclear genome and mtDNA for ETC biogenesis. Additional network analyses on the recovered hits using published DNA binding profiles illustrated potential regulatory connections and a complex hierarchy of the transcription regulations on mitochondrial biogenesis. The combination of genetic and bioinformatic analyses also facilitated the identification of YL-1 as an upstream regulator of CG1603.

Results

The design of a genetic modifier screen for genes regulating mtDNA maintenance and expression

Mutations on nuclear-encoded ETC genes block cell cycle and disrupt the differentiation and morphogenesis of developing eyes (Mandal et al., 2005; Owusu-Ansah *et al*., 2008). RNAi against *tfam* or *myc*, which promotes the expression of ETC genes encoded on mtDNA and nuclear genome, respectively, also reduced adult eye size (**Figure 1A**). These observations prompted us to use fly eye as a model to identify transcription factors regulating ETC biogenesis. However, inhibitions of any genes essential for cell viability, proliferation, or differentiation, exemplified by RNAi targeting a mitotic cyclin, *CycB* (**Figure 1A**), would disrupt eye development. Therefore, assaying eye morphology alone is not sufficient to enrich candidates regulating ETC biogenesis.

The mitochondrial genome of wt *Drosophila melanogaster* contains a single XhoI site. The expression of a mitochondrially targeted restriction enzyme, XhoI (MitoXhoI) in *Drosophila* ovary effectively selects for escaper progeny carrying mtDNA mutations that abolish the XhoI site (Xu *et al*., 2008). In a heteroplasmic background containing both wild type and XhoI resistant genome (*XhoI*), the expression of MitoXhoI can effectively remove the wild type genome and hence generate mtDNA deficiency (Chen *et al*., 2015). As a result, the adult eyes were slightly smaller than the control (**Figure 1A**). Considering that mtDNA encodes core components of ETC, we

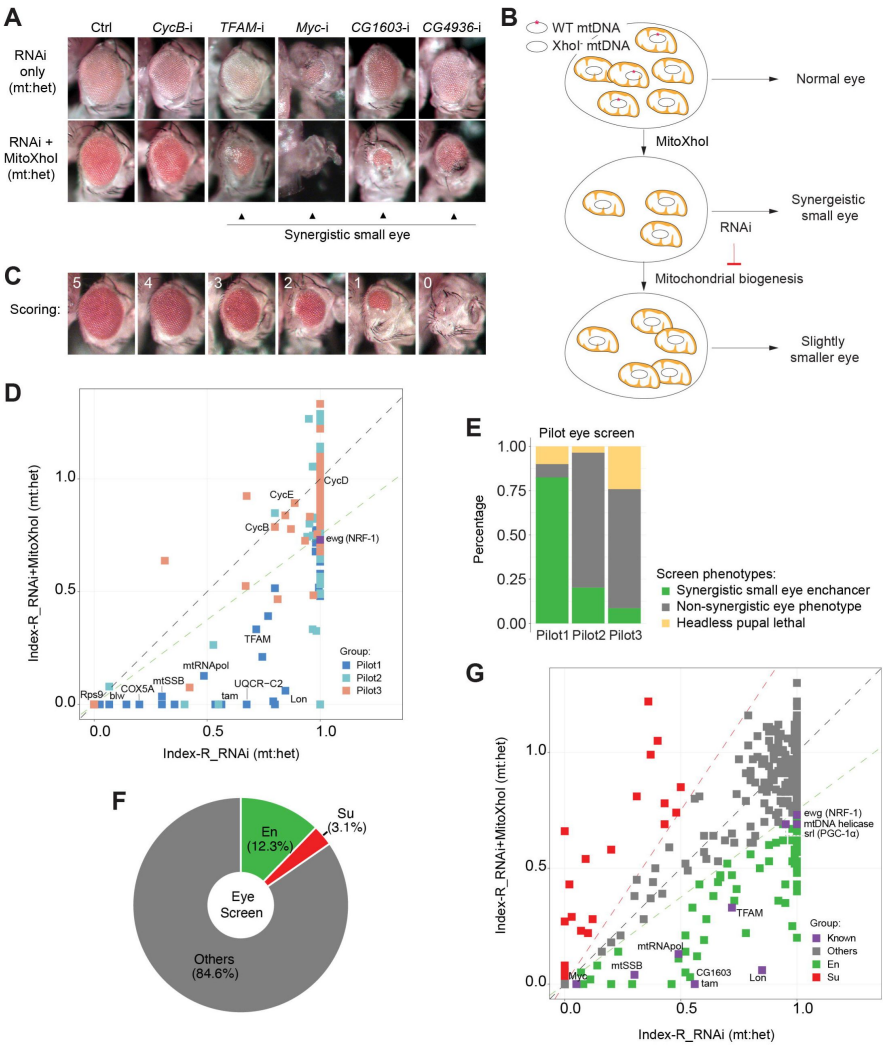

Figure 1.

A genetic modifier screen identifying transcription factors regulating ETC biogenesis.

(A) Representative images of adult eye for the control RNAi (Ctrl) and RNAi of selected genes tested in the eye screen, including *CycB* RNAi (*CycB*-i), *TFAM* RNAi (*TFAM*-i), *Myc* RNAi (*Myc*-i), *CG1603* RNAi (*CG1603*-i) and *CG4936* RNAi (*CG4936*-i). The upper panel shows eyes from RNAi-only offspring and lower panel displays eyes from RNAi+MitoXhoI offspring cultured at the same condition. Arrowheads indicate the synergistic small eye phenotype resulting from the combination of gene knockdown and the mtDNA deficiency caused by mitoXhoI in the background of heteroplasmic mtDNAs. (B) Schematic of the genetic modifier screen methodology (see text for details). (C) Representative images illustrating the scoring of eye size. (D) A plot illustrating the calling of positive hits in the pilot screen. Each datapoint represents the Index-R of RNAi (X values) or RNAi+MitoXhoI flies (Y values) for each gene belonging to the different groups (see **Figure 1E** and *Supplementary file 1* for details). Genes with datapoints lie below the grey diagonal dash line exhibited a synergistic effect when combining their RNAi with mtDNA deficiency suggesting a potential role in regulating ETC biogenesis. The datapoint for *ewg*, the fly homolog of *NRF-1*, is labeled in purple. The green dashed line of slope 0.75 outlines the threshold for calling out positive hits based on *ewg*'s performance in the screen. (E) Graph summarizing the pilot screen of nuclear-encoded genes, demonstrating the efficacy of this screen in identifying genes involved in mitochondrial ETC biogenesis. Pilot group 1 (Pilot1) has 40 genes that are either nuclear-encoded ETC subunits or related to mtDNA maintenance and gene expression (Mito-EBR). Pilot2 has 84 genes involved in other mitochondrial processes. Pilot3 has 58 essential genes from other cellular components. (F) Graph summarizing the percentages of synergistic enhancers (En) and suppressors (Su) identified in the screen (see **Figure 1G** and *Supplementary file 1* for details). (G) A plot illustrating the calling of positive hits in the screen of TF genes. Factors that are known to be involved in mitochondrial or ETC biogenesis are marked in purple (Known). The green dashed line outlines the threshold for calling out synergistic enhancers (En, green square). The red dashed line of slope 1.5 outlines the threshold for calling out suppressors (Su, red square).

reasoned that inhibiting a gene related ETC biogenesis would have synergistic effect with the mtDNA deficiency on eye development, and the combination of these two genetic manipulations should lead to a stronger disruption of eye development than either of these conditions individually (**Figure 1A, B**). On this basis, we devised a scheme of modifier screen in eye for genes involved in ETC biogenesis (**Figure 1B**).

The RNAi modifier screen identifying transcription factors regulating ETC biogenesis

To assess the efficacy of this scheme, we carried out a pilot RNAi screen, covering 124 nuclear-encoded mitochondrial genes and 58 non-mitochondrial genes annotated in various cellular processes (**Figure 1C-E**, and *Supplementary file 1*). In practice, male flies carrying a *UAS-IR* transgene were crossed with *Sco/CyO, mitoXhoI; eyeless-GAL4* heteroplasmic female flies (carrying both wild type and *XhoI*$^{-}$ mtDNA). This cross generated two groups of offspring, RNAi-only and RNAi together with MitoXhoI expression (RNAi+MitoXhoI) that were cultured in a same vial, thereby minimizing any potential discrepancy caused by environmental factors. Most RNAi flies survived to adult stage but had reduced eye size. A few RNAi flies were lethal at pupae stage, due to a lack of head capsule that is derived from the eye antenna disc.

For most genes tested in the pilot screen, eyes of RNAi+MitoXhoI flies were smaller than the corresponding RNAi-only flies. To rule out a simple additive effect between RNAi and MitoXhoI expression, we carried out additional analyses to semi-quantify a potential synergy between RNAi intervention and mtDNA deficiency caused by MitoXhoI expression. The eye size of progeny was arbitrarily scored on a scale from 0 to 5 (**Figure 1C**). The indexes of eye size reduction (Index-R) of RNAi and RNAi+MitoXhoI flies were calculated by normalizing the mean eye size scores of each genotype to the corresponding values of control RNAi or control RNAi+MitoXhoI, respectively, and were subsequently plotted against each other on a linear graph (**Figure 1D**). If a RNAi intervention had synergistic effect with mtDNA deficiency, it would lie below the diagonal line. We also included *ewg*, the fly homolog of *NRF-1*, in the pilot screen to set the threshold for calling out positive hits. Of total 40 genes that are related to ETC biogenesis (Mito-EBR) including ETC subunits, mitochondrial protein import and membrane insertion machinery, ETC assembly factors, and proteins related to the expression of mtDNA-encoded ETC subunits, 82.5% (33 genes) emerged as enhancers (**Figure 1E**). The proportions of synergistic enhancers were much lower in the group of genes involved in other mitochondrial processes (20.2%) or groups of other essential genes not related to mitochondria (8.6%), indicating the efficacy of this modifier screen in enriching genes related to ETC biogenesis (**Figure 1E**).

To understand transcriptional regulations of ETC biogenesis, we screened 1264 RNAi lines that cover 638 genes annotated as transcriptional regulators in *Drosophila* genome. Total 77 enhancers were identified (**Figure 1F, G** and *Supplementary file 1*), including all known factors involved in ETC biogenesis such as Myc, TFAM (Scarpulla, 2008; Wang et al., 2019). We also recovered 20 suppressors, of which, eyes of RNAi+MitoXhoI flies were larger than the corresponding RNAi-only flies.

Regulatory network of mitochondrial biogenesis

Among 77 TFs identified in the initial modifier screen, 49 TFs have ChIP-seq data available in modERN (Kudron *et al*., 2018). To further understand the transcriptional regulation of ETC biogenesis, we performed the network analysis on these 49 TFs using the *"vertex sort"* algorithm (Jothi et al., 2009), and constructed a regulatory network (**Figure 2A** and *Supplementary file 2*). All 49 TFs had binding sites on the promoter region of at least one nuclear mitochondrial gene (**Figure 2B**, **Figure 2—figure supplement** and *Supplementary file 3*). Respectively, 89% nuclear-encoded mitochondrial genes (851), including nearly all Mito-EBR genes (*Supplementary file 3),* were bound by at least one TF. Given that 28 hits were not included in the analyses due to a lack of ChIP-seq data, the actual coverage of total 77 TFs on nuclear mitochondrial genes would be

more comprehensive. Six TFs bound to more than half of mitochondrial genes (**Figure 2B**, **Figure 2—figure supplement** and *Supplementary file 3*). However, not a single TF covered all mitochondrial genes, or all genes in a specific mitochondrial process, which is consistent with the diverse evolution origin of mitochondrial genes (Kurland and Andersson, 2000). It also indicates that there is no such a "master" regulator controlling all aspects of mitochondrial genesis. Forty-seven TFs were identified as strongly connected component due to their extensive connections and were classified in the core or bottom layer of the hierarchical structure, suggesting complexed co-regulations and potential redundancy among these TFs in controlling mitochondrial biogenesis (**Figure 2A** and *Supplementary file 2*). Through this interconnected network, every single node can link to all 851 mitochondrial genes in the coverage. Two transcription factors, Crg-1 and CG15011 were identified as the top-layer TFs with no upstream regulators in the network (**Figure 2A** and *Supplementary file 2*). Crg-1 is a circadian regulated gene (Rouyer et al., 1997). CG15011 is an X-box binding protein and had a binding profile to another X box binding protein, Xbp1 (*Supplementary file 3)*, a stress respondent and regulator (Acosta-Alvear et al., 2007). These top-layer TFs may sense physiological oscillations and stresses to modulate mitochondrial biogenesis through the underlying network. Additionally, YL-1 and E(bx), two components in the middle layer, are involved in chromatin-remodeling (Liang et al., 2016; Wysocka et al., 2006), suggesting a potential regulation of mitochondrial biogenesis at a chromatin level.

CG1603 regulates ETC gene expression and mitochondrial biogenesis

To validate the efficacy of this integrated genetic and bioinformatic approach, we next followed up on *CG1603*, one of the strongest hits from the primary screen (**Figure 1A, G**) and exhibited binding to a diverse array of genes associated with ETC biogenesis (**Figure 2B**, **Figure 2—figure supplement** and *Supplementary file 3*). *CG1603* RNAi slightly reduced eye size. However, the combination of *CG1603* RNAi with MitoXhoI expression in the heteroplasmic background resulted in markedly smaller eyes, indicating a clear synergy between the inhibition of *CG1603* and the mtDNA deficiency. We next asked whether CG1603 was involved in mtDNA maintenance. The *Drosophila* midgut is essentially a monolayer epithelium and composed of intestine stem cells, enteroblasts, enteroendocrine cells and enterocytes (EC). The large, flattened enterocytes allow high-resolution imaging of mitochondria and mitochondrial nucleoids. Additionally, the simple organization and distinct cell types, containing both proliferative and terminally differentiated cells, render the midgut an ideal model to evaluate the impact of mitochondrial disruptions on cell proliferation and differentiation (Zhang et al., 2020). We used a "flip-out" method to activate *CG1603* RNAi in a subset of cells (Prober and Edgar, 2000; Zhang *et al*., 2020), and imaged TFAM-GFP (Zhang et al., 2016), a marker for mitochondrial nucleoids in midgut clones. Both the total TFAM-GFP level and the number of mtDNA nucleoids (TFAM puncta), were markedly reduced in *CG1603* RNAi clones (**Figure 3A-C**), suggesting that CG1603 is necessary for maintaining the steady-state level of mtDNA. We constructed a *SDHA-mNG* reporter line by inserting the *mNeonGreen (mNG)* cDNA in-frame, downstream of the endogenous locus of *SDHA*, a subunit of ETC Complex II that are entirely encoded by the nuclear genome. SDHA-mNG level was notably reduced in *CG1603* RNAi clones (**Figure 3D, E**), suggesting that CG1603 is also required for the expression of nuclear-encoded ETC subunits. Different from TFAM-GFP that marks mitochondrial nucleoids and appears as puncta in mitochondria (Chen et al., 2020), SDHA-mNG uniformly distributed in the mitochondrial matrix (**Figure 3D**). By quantifying the total volume of SDHA-mNG positive voxels in the 3-D rendering, we found that the total mitochondrial volume was also reduced in *CG1603* RNAi clones (**Figure 3F**). Collectively, these results demonstrate that CG1603 regulates the expression of genes essential for both ETC function and mitochondrial biogenesis. *CG1603* RNAi produced very few EC clones (**Figure 3A, D** and **Figure 3—figure supplement**), consistent with the notion that mitochondrial respiration is necessary for ISCs differentiation (Zhang *et al*., 2020).

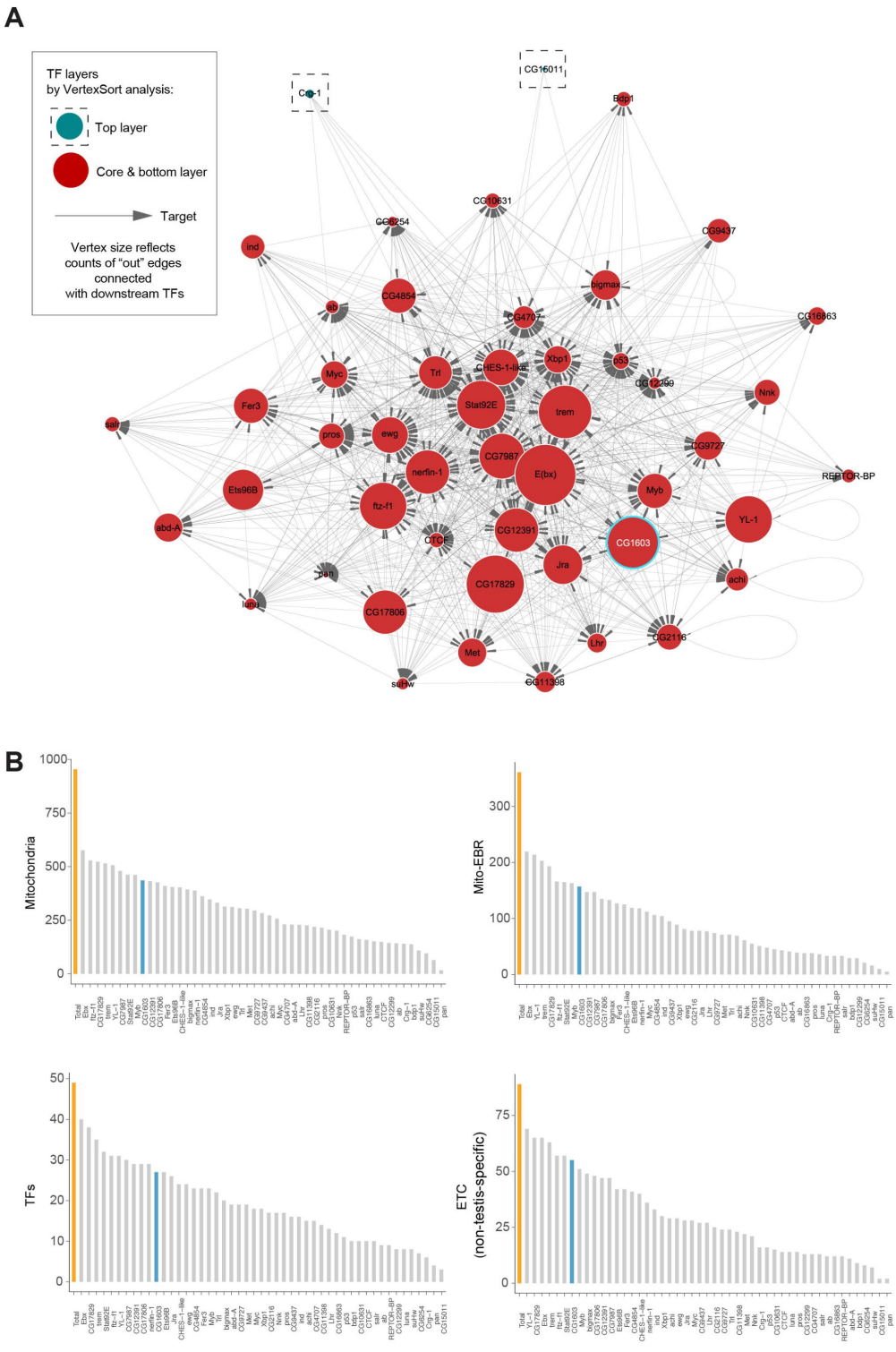

Figure 2.

Regulatory network of mitochondrial biogenesis.

(A) The potential transcriptional regulatory network of nuclear-encoded mitochondrial genes. (B) Bar graphs illustrating the promoter binding profiles of the 49 synergistic enhancer TFs within different groups of genes (nuclear-encoded mitochondrial genes, Mito-EBR genes, 49 synergistic enhancer TFs and ETC genes). Total gene number of the group (orange) and the number bound by CG1603 (cyan) were highlighted.

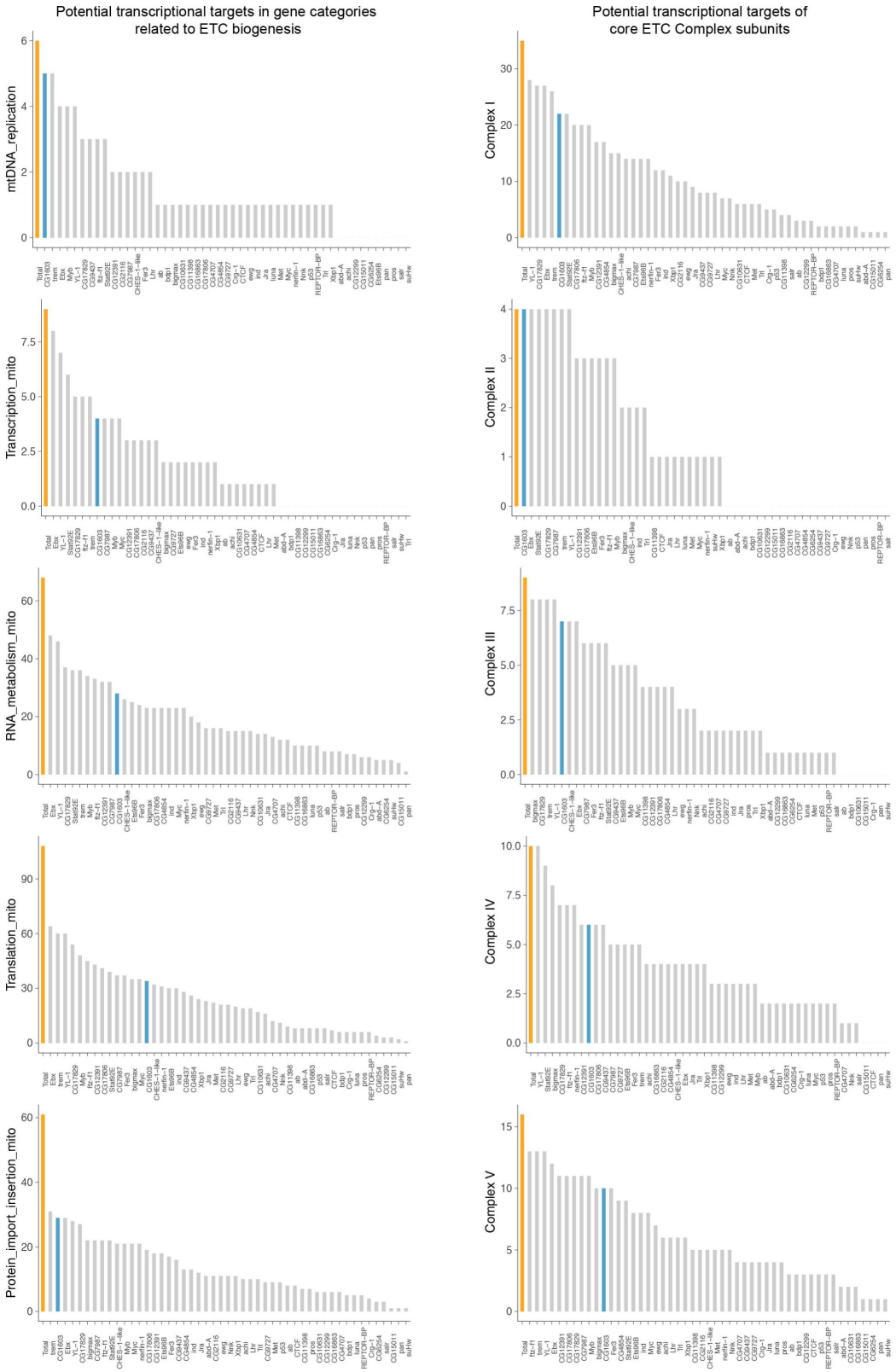

Figure 2—figure supplement.

Bar graphs summarizing the promoter binding profiles of the 49 synergistic enhancer TFs within subgroups of genes involved in different processes of ETC biogenesis. Total gene number of the subgroup (orange) and the number bound by CG1603 (cyan) were highlighted.

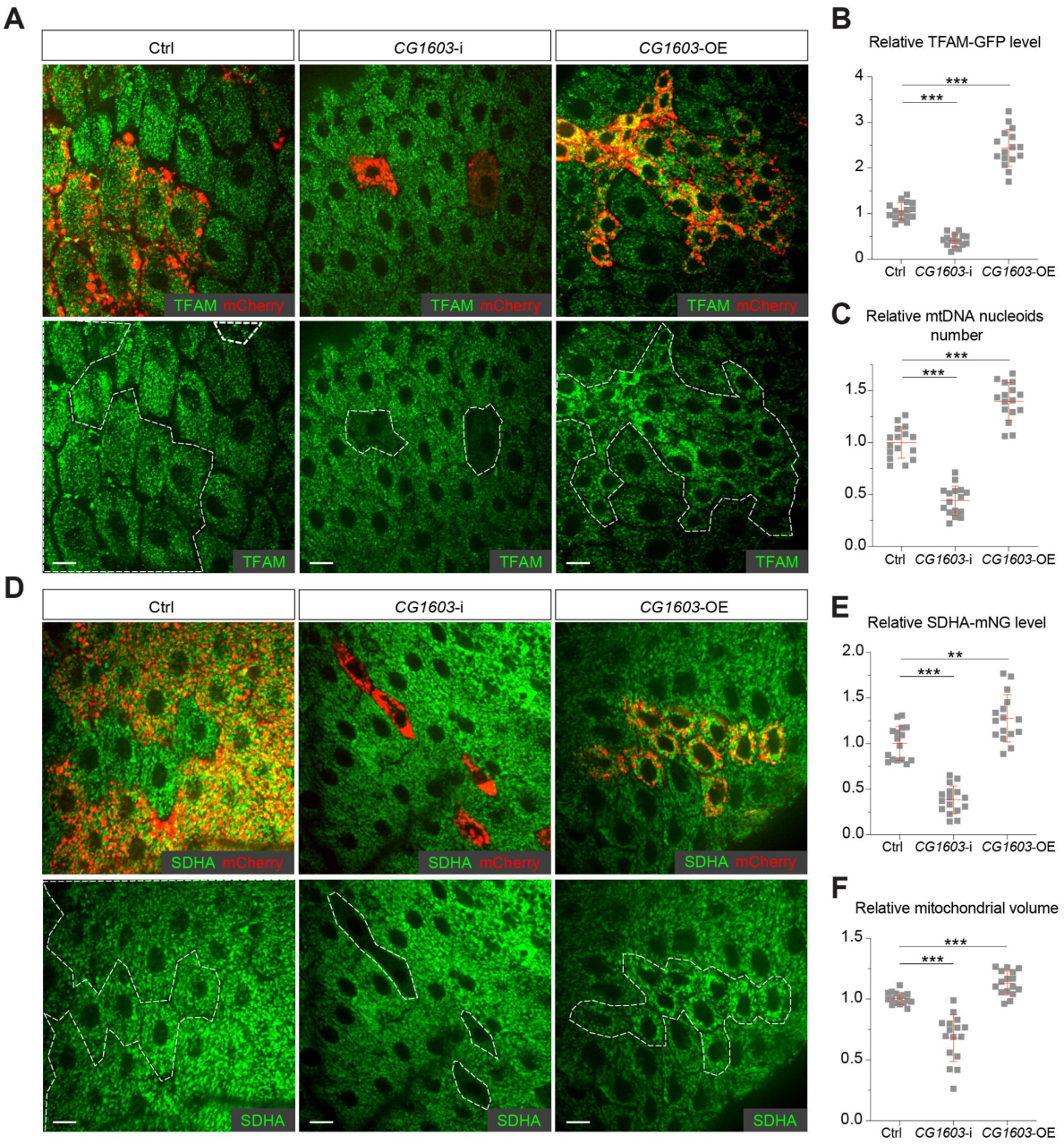

Figure 3.

CG1603 promotes ETC gene expression and mitochondrial biogenesis.

(A, D) Representative images of control RNAi (Ctrl), *CG1603* RNAi (*CG1603-i) and CG1603* overexpression (*CG1603*-OE*)* midgut EC clones with endogenously expressed TFAM-GFP (A) or SDHA-mNG (D) visualized in green. Clones were labeled by mCherry red and compared with wt neighbors. White dash lines aided in illustrating clones. Scale bars: 10 μm. (B, C, E, F) Quantification of the relative TFAM-GFP level (B), the relative mtDNA nucleoids number (C), the relative SDHA-mNG level (E), and the relative mitochondrial volume (F) in the EC clones to their wt neighbors. n=16 from 8 midguts for each group, error bar: SD. **: p<0.01, ***: p<0.001.

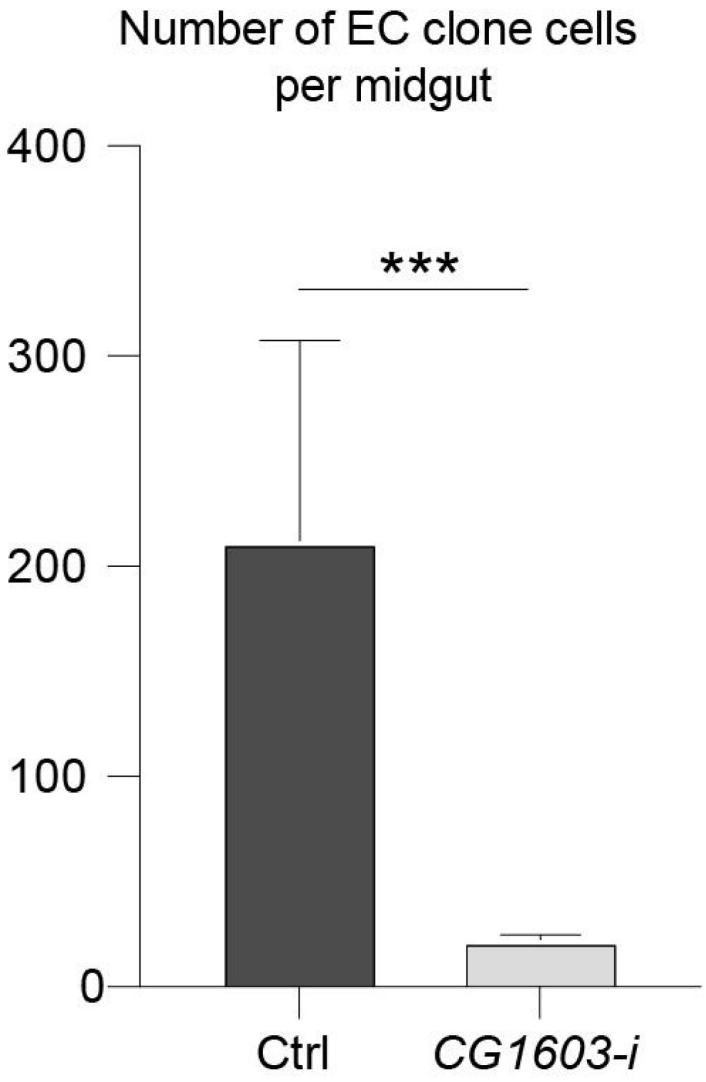

Figure 3—figure supplement.

Number of EC clone cells in control RNAi (Ctrl) and *CG1603* RNAi (*CG1603*-i) midguts. n= 8, error bar: SD. ***: p<0.001.

CG1603 regulates cell growth and differentiation

CG1603 encodes a C2H2 zinc finger protein. It has one C2H2 Zinc finger (C2H2-ZF) at its N-terminus, followed by two MADF (myb/SANT-like domain in Adf-1) domains, and six additional zinc fingers at the C-terminus (**Figure 4A, B**). A PiggyBac transgene, *PBac[SAstopDSRed]LL06826* is inserted between the exons 2 and 3 of *CG1603* locus. This modified Piggybac mutator transgene contains splicing donors and stop codons in all 3 reading frames (Schuldiner et al., 2008), and thereby would disrupt the translation of the full length CG1603 protein. Homozygous *PBac[SAstopDSRed]LL06826* was lethal, arrested at the 2nd instar larval stage and eventually died after 10 days (**Figure 4C**). Both the steady state level of mtDNA, and total mitochondrial mass assessed by the levels of several mitochondrial proteins were reduced in these larvae (**Figure 4D, E**), as well as the integrities and activities of ETC complexes (**Figure 4—figure supplement A**). The lethality of this PiggyBac transgene was mapped to a genomic region spanning the *CG1603* locus (**Figure 4—figure supplement B**, *C*). Importantly, a *P[CG1603^{gDNA}]* transgene that covers the genomic region of *CG1603* fully rescued its viability (**Figure 4A, F**). These results demonstrate that the lethality of *PBac[SAstopDSRed]LL06826* was caused by the loss of function of CG1603, and we hence named it *CG1603^{PBac}* thereafter. Using FLP/FRT-mediated recombination, we generated homozygous *CG1603^{PBac}* mutant clones in both germline and follicle cells in adult ovaries. Consistent with the results of "flip-out" RNAi experiments in the midgut, both the total TFAM level and the number of mtDNA nucleoids, visualized by an endogenously expressed TFAM-mNG reporter, were significantly reduced in *CG1603^{PBac}* clones (**Figure 5A-D** and **Figure 5—figure supplement A, B**). In most *CG1603^{PBac}* clones, TFAM-mNG puncta were hardly observed, demonstrating an essential role of CG1603 in mtDNA maintenance. Compared to twin clones, *CG1603^{PBac}* follicle cell clones contained significantly fewer cells, and these cells were smaller, indicating that CG1603 promotes both cell growth and cell proliferation (**Figure 5A, E**). *CG1603^{PBac}*egg chambers were also notably small, even smaller than the adjacent anterior egg chambers that are at earlier developmental stages in the same ovariole (**Figure 5A**). We assessed $\Delta\psi_m$ using the ratiometric imaging of TMRM and MitoTracker Green (Zhang et al., 2019). $\Delta\psi_m$ was nearly abolished in *CG1603^{PBac}*clones with reduced MitoTracker Green staining (**Figure 5F** *and* **Figure 5-figure supplement A**). All together, these observations demonstrate that CG1603 promotes mitochondrial biogenesis and is essential for ETC biogenesis.

CG1603 is a transcription factor regulating nuclear mitochondrial gene expression

CG1603 protein exclusively localized to nucleus when expressed in cultured cells (**Figure 6A**). We generated a transgene expressing CG1603-mNG fusion protein by inserting *mNeonGreen* cDNA into the endogenous locus of *CG1603*. CG1603-mNG localized to nuclei in ovaries (**Figure 6B**) and directly bound to polytene chromosomes in salivary gland (**Figure 6C**). Notably, CG1603-mNG was highly enriched on less condensed chromatin regions that had weak Hoechst staining (**Figure 6C**). We performed RNA sequencing (RNA-seq) in larvae to uncover potential targets of CG1603. Between wt and *CG1603^{PBac}*larvae, total 7635 genes were differentially expressed, including 86% nuclear-encoded mitochondrial genes (**Figure 6D** and *Supplementary file 4, 5*). Nearly half of nuclear-encoded mitochondrial genes were among 1698 genes that were reduced by more than 2-folds in *CG1603* mutant (**Figure 6E** and *Supplementary file 5a*), including many structural subunit genes of all five ETC complexes (*Supplementary file 5b*), some of which were further confirmed by quantitative real-time PCR (**Figure 6F**). Gene Ontology (GO) enrichment analyses on these 1698 genes also revealed that all top ten significantly enriched biological processes were related to mitochondria, including “mitochondrial translation”, “mitochondrial gene expression”, “electron transport chain”, “aerobic respiration”, “cellular respiration” and “ATP metabolic process” (**Figure 6G**).

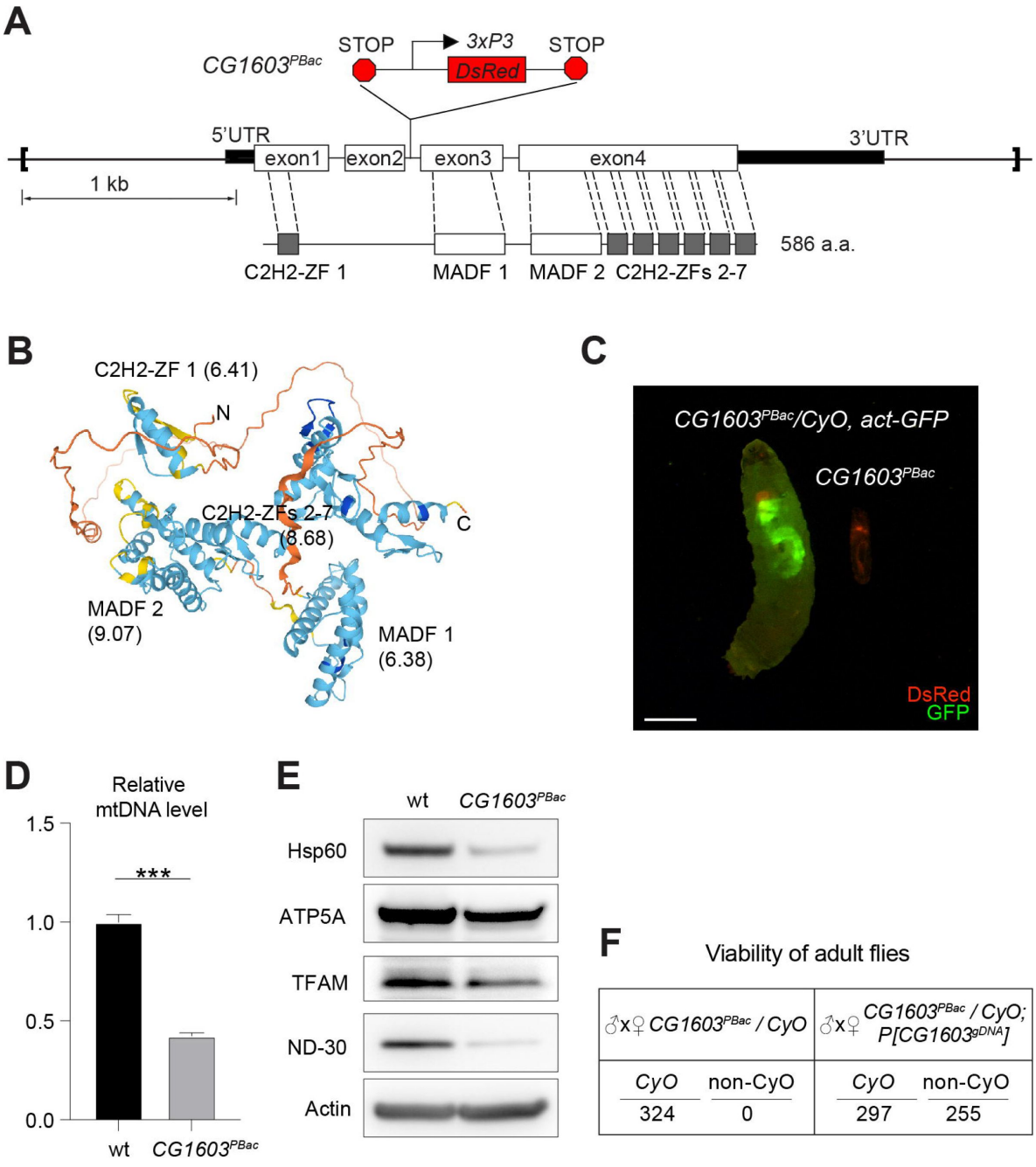

Figure 4.

***CG1603* gene model, product, mutant and the genomic DNA transgene.**

(A) Schematic representation of *CG1603* genomic locus, showing the *CG1603* transcript (5' and 3'UTR in black bar and four exons in white), its protein product (586 amino acids in length, and characterized by seven C2H2-ZF and two MADF domains), the $CG1603^{PBac}$ mutant allele (with a piggyBac insertion in the second intron, which is marked by fluorescent DsRed driven by an eye-specific *3xP3* promoter and flanked by stop codons in all three reading frames terminating translation through downstream), and the genomic region (in square brackets, from 955 bp upstream of the *CG1603* 5'UTR to 656 bp downstream of *CG1603* 3'UTR) used for $P[CG1603^{gDNA}]$ transgene. (B) Predicted 3D structure of the CG1603 protein by AlphaFold. Labels indicate the N-and C-terminus, as well as the specific protein domains along with their predicted isoelectric point (pI). (C) Images of $CG1603^{PBac}$ / *CyO, Act-GFP* and homozygous $CG1603^{PBac}$ larvae cultured together at 25°C, day 4 after egg laying. Green: GFP; Red: DsRed. Scale bars: 1 mm. (D) Relative mtDNA levels in $CG1603^{PBac}$ mutant larvae to wild type (wt) control. n= 3, error bar: SD. ***: p<0.001. (E) Western blots of mitochondrial proteins in $CG1603^{PBac}$ mutant larvae to wild type (wt) control. (F) $P[CG1603^{gDNA}]$ restored viability of $CG1603^{PBac}$flies. The number of progenies for each genotype is listed.

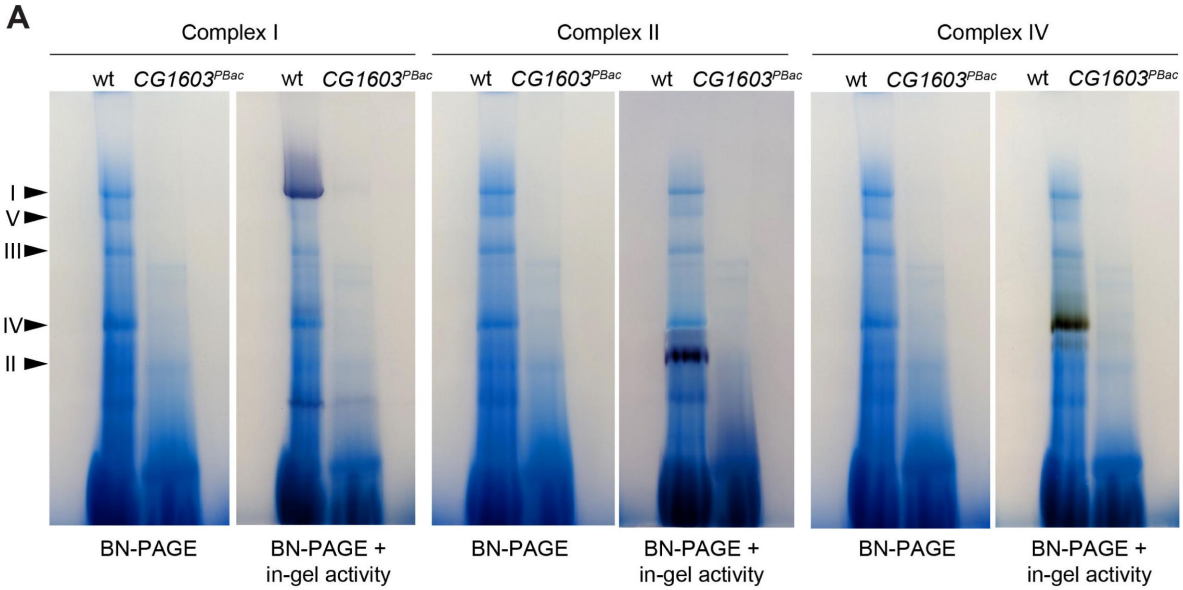

B

Genotype	Phenotype	with *P[CG1603^{gDNA}]* transgene
CG1603^{PBac} / *CG1603^{PBac}*	Lethal	Viable
CG1603^{PBac} / *Def ^{k08815}*	Lethal	Viable
CG1603^{PBac} / *Def ^{Exel6052}*	Lethal	Viable
CG1603^{PBac} / *Def ^{Exel6053}*	Viable	

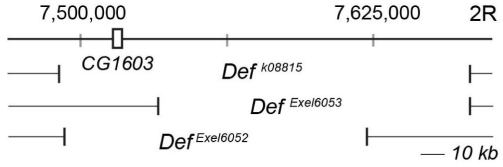

Figure 4-figure supplement

Figure 4—figure supplement A. Blue native PAGE and in-gel activity analyses of ETC Complex I, II & IV isolated from wild type (wt) and *CG1603^{PBac}* mutant. An equal amount of protein was used for each sample.
Figure 4—figure supplement B. Summary of adult viability phenotypes of combinations of *CG1603^{PBac}* mutant, *P[CG1603^{gDNA}]* transgene and deficiency chromosomes.
Figure 4—figure supplement C. Schematic map of deficiency chromosomes spanning *CG1603* genomic region.

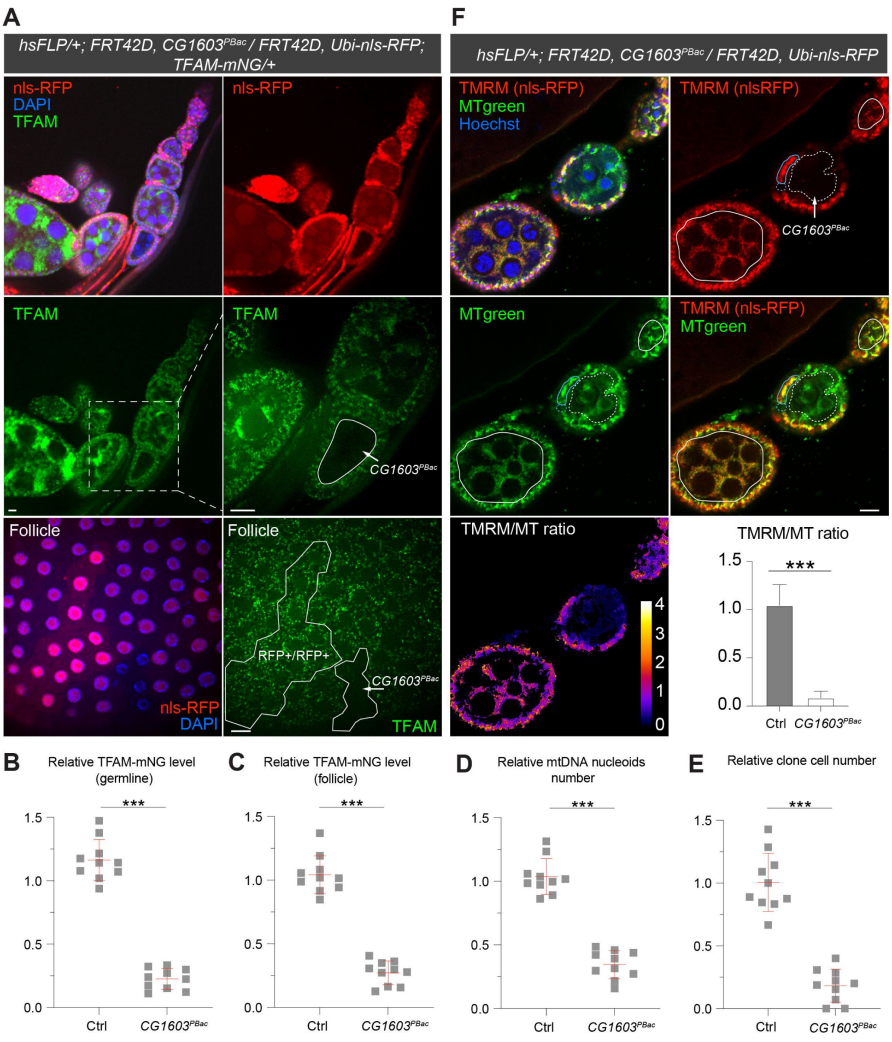

Figure 5.

Clonal analyses confirmed CG1603's role in mitochondrial biogenesis and activity.

(A) Representative images of *CG1603*^{PBac} mutant germline (top and middle panel) and follicle (bottom panel) clones in late-stage egg chambers of adult ovaries with endogenously expressed TFAM-mNG visualized in green. Homozygous mutant clones were marked by the absence of RFP and compared with either flanking RFP-positive cysts (germline) or homozygous wt twin (follicle). White dash lines aided in illustrating clones. The wt (RFP+/RFP+) follicle clone showed markedly higher RFP intensity than the heterozygous (RFP+/RFP-) cells, also see **Figure 5—figure supplement B**. Red: nls-RFP; Blue: DAPI. Scale bars: 10 μm. (B) Quantification of the relative TFAM-mNG level in the homozygous *FRT42D* control and *CG1603*^{PBac} mutant germline clones in early-stage egg chamber to their anterior flanking RFP-positive cysts within the same ovariole. also see **Figure 5—figure supplement A**. n=10 for each group, error bar: SD. ***: p<0.001. (C-E) Quantification of the relative TFAM-mNG level (C), the relative mtDNA nucleoids number (D) and the relative clone cell number (E) in the homozygous *FRT42D* control and *CG1603*^{PBac} mutant follicle clones to their wt twins. n=10 for each group, error bar: SD. ***: p<0.001. (F) TMRM / MitoTracker Green (MT) ratiometric live imaging and quantification of ovarioles containing homozygous *CG1603*^{PBac} mutant germline clones (highlighted by white dash lines). Notably, in contrast to flanking control cysts (highlighted by white lines), $\Delta\psi_m$ was almost absent in mutant clones. Please note that compared to TMRM, nls-RFP signal was too low to be detected in ratiometric imaging. Nonetheless, the nls-RFP was readily detected in control cysts, but not in homozygous *CG1603*^{PBac} clones, *via* visual observation, as depicted in **Figure 5A** and **Figure 5—figure supplement**. A twin pair of follicle clones in the same egg chamber were also highlighted (cyan line for control and cyan dash line for homozygous *CG1603*^{PBac} mutant). The MT intensity was reduced in both the germline and follicle *CG1603*^{PBac}clones, compared to germ cells in adjacent egg chambers and follicle cells in the same egg chamber, respectively. Quantification with background correction for MT intensity in germline clones is shown in **Figure 5—figure supplement C**. Blue: Hoechst. Scale bars: 10 μm. n= 8, error bar: SD. ***: p<0.001.

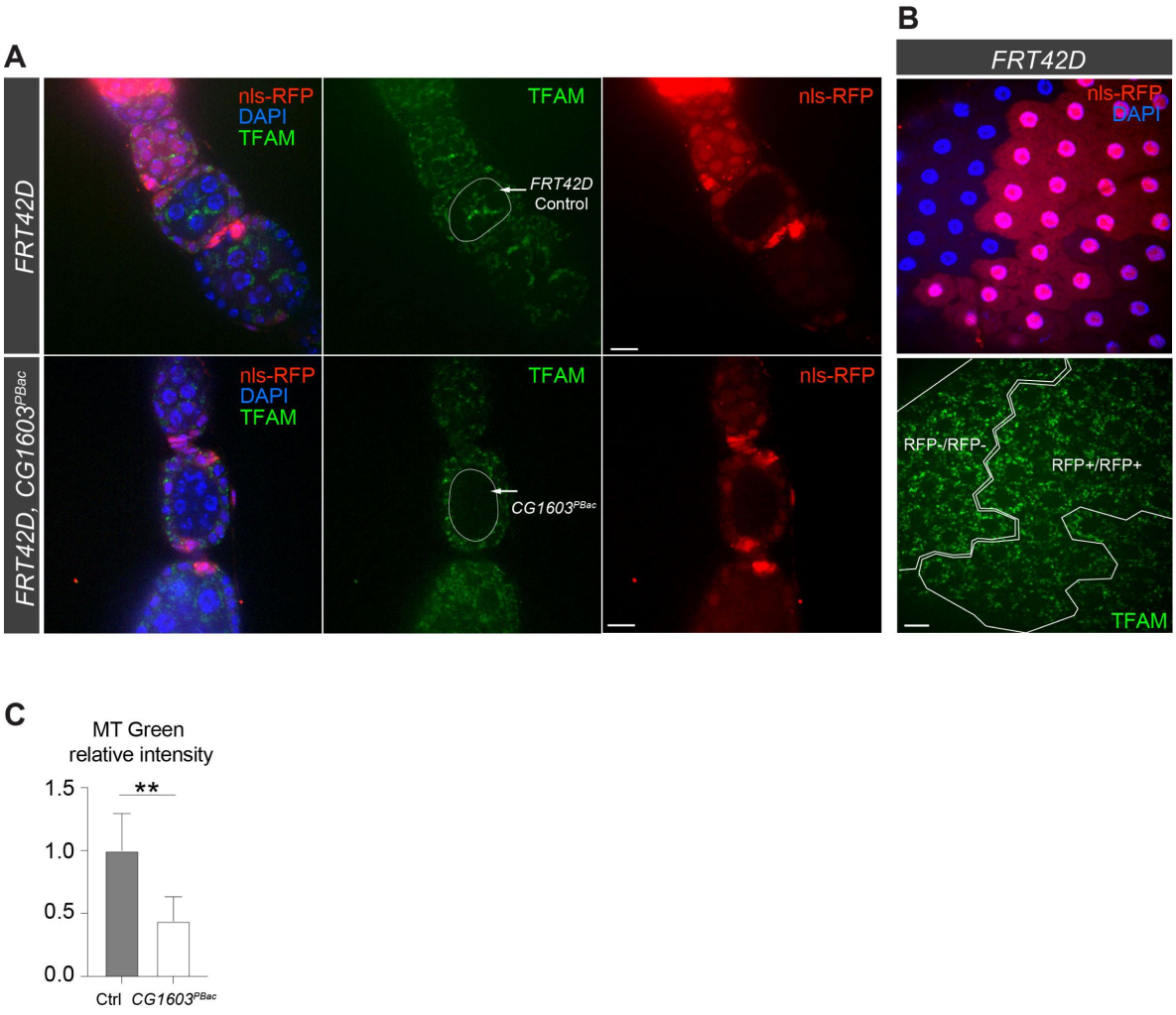

Figure 5-figure supplement

Figure 5—figure supplement A. Representative images of homozygous *FRT42D* control and *CG1603*^{PBac} mutant germline clones in early-stage egg chambers of adult ovaries with endogenously expressed TFAM-mNG visualized in green. Homozygous mutant clones were marked by the absence of RFP and compared with flanking RFP-positive cysts. Red: RFP; Blue: DAPI. Scale bars: 10 μm.

Figure 5—figure supplement B. Representative images of homozygous *FRT42D* control follicle cell clone (RFP-/RFP-) and its wt twin (RFP+/RFP+) with endogenously expressed TFAM-mNG visualized in green. Red: nls-RFP; Blue: DAPI. Scale bars: 10 μm.

Figure 5—figure supplement C. The relative intensity of MitoTracker (MT) Green in *CG1603*^{PBac} mutant germline clones to control (Ctrl). n= 8, error bar: SD. **: p<0.01. Related to **Figure 5F**.

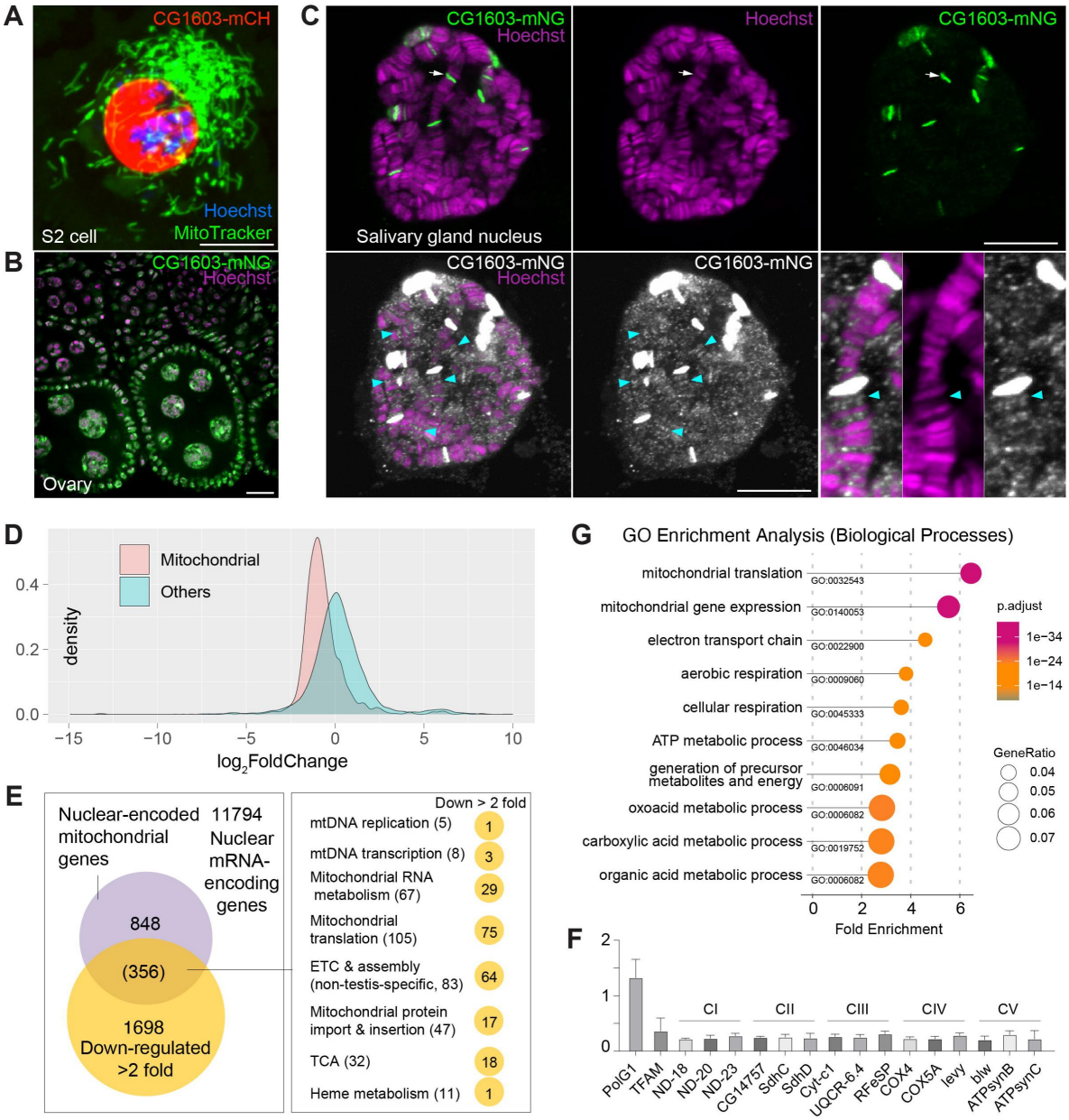

Figure 6.

CG1603 localizes in the nucleus and is essential for regulating nuclear mitochondrial gene expression.

(A-B) Representative images showing nuclear localization of CG1603 protein in cultured S2 cell (A) and adult ovary (B). Green: MitoTracker Green in S2 cell, and CG1603-mNG in tissues; Red: CG1603-mCH; Blue & Magenta: Hoechst. Scale bars: 10 μm. (C) Representative images showing bindings of endogenously expressed CG1603 proteins to less condensed euchromatin regions in the polytene chromosomes of salivary gland. High intensity CG1603-mNG bands were visualized in green in upper panel as indicated by arrow, and low intensity bands were visualized in white in lower panel as indicated by arrow heads with image B&C adjusted. Magenta: Hoechst. Scale bars: 10 μm. (D) Density plot illustrating the distribution of expression changes of the nuclear-encoded mitochondrial and non-mitochondrial genes in *CG1603*^{PBac}mutant. (E) Graph illustrating the overlap between nuclear-encoded mitochondrial genes and differentially expressed genes (DEGs) that down-regulated > 2-fold, as well as the distribution of the overlapped genes in different mitochondrial function categories. (F) Relative mRNA levels of several ETC biogenesis-related genes in *CG1603*^{PBac} mutant larvae to control, measured by real-time PCR. n= 3, error bar: SD. (G) Gene Ontology (GO) enrichment analyses of DEGs that down-regulated > 2-fold. The top 10 enriched biological processes are shown.

CG1603 had 8963 binding sites (peaks) distributing over all four chromosomes (**Figure 7A** and *Supplementary file 6*). A subset of peaks showed high intensity evaluated by signalValue (**Figure 7A** and *Supplementary file 6*), which may correspond to these high intensity CG1603-mNG bands on the polytene chromosomes of salivary gland (**Figure 6C**). Most CG1603 binding sites (6799) were found at promoter regions, close to the transcription start site (**Figure 7B**, *C* and *Supplementary file 6*), which is a key feature of a typical TF. Using the RSAT "peak-motifs" tool (Thomas-Chollier et al., 2012), an 8-bp palindromic sequence, "TATCGATA" emerged as the most prevalent CG1603 binding motif (**Figure 7D** and *Supplementary file 7*). CG1603 bound to the genomic regions of 50% nuclear-encoded mitochondrial genes, and among these genes, 79.5 % were down-regulated in the $CG1603^{PBac}$ mutant (**Figure 7E** and *Supplementary file 6)*, indicating a great accordance between ChIP data and RNAseq results. Most nuclear-encoded mitochondrial genes that were both bound by CG1603 and down-regulated in *CG1603* mutant were ETC genes or related to ETC biogenesis (**Figure 7F** and *Supplementary file 6)*. Collectively, CG1603 appears to be essential for mitochondrial biogenesis and coordinates the expression of both nuclear and mtDNA genes in ETC biogenesis.

The integrated approach identifies YL-1 as an upstream regulator of CG1603

In the network analyses, CG1603 was positioned in the middle layer, linked to 7 TFs above and 6 TFs below by integrating the RNA-seq result with ChIP-seq data (**Figure 8A**). Through these TFs below, CG1603 may indirectly control the expression of 2230 genes, including 291 mitochondrial genes downregulated in $CG1603^{PBac}$ but not bound by CG1603 (**Figure 7E**). Using the "flip-out" RNAi system in the midgut, we found that among 7 TFs upstream of CG1603 in the network, E(bx), YL-1, trem, STAT92E and Myb were also required for maintaining TFAM levels (**Figure 8—figure supplement A, B**). To further verify their potential roles in regulating CG1603, we performed RNAi against these genes in midgut clones carrying CG1603-mNG reporter. Only *YL-1* RNAi clones displayed a markedly reduction of CG1603 protein compared with neighboring cells (**Figure 8B, C**). Furthermore, overexpression of CG1603 restored eye size, TFAM-GFP, SDHA-mNG and mtDNA levels cause by *YL-1* RNAi (**Figure 8D-J** *and* **Figure 8—figure supplement C**). These results indicate that YL-1 is indeed an upstream regulator of CG1603, and through which to regulate ETC biogenesis.

Discussion

The dual genetic control of mitochondria presents a fundamental challenge: how are the nuclear genome and mitochondrial DNA coordinated to ensure the efficiency and integrity of oxidative phosphorylation system and other critical mitochondrial processes? In *Drosophila* ovary, the mitochondrial A-kinase-anchor-protein, MDI promotes the translation of a subset of nuclear mitochondrial proteins by cytosolic ribosomes on the mitochondrial outer membrane (Zhang *et al*., 2016). MDI's targets are predominantly ETC subunits and proteins essential for mitochondrial genome maintenance and gene expression (Zhang *et al*., 2019). This mechanism coordinates the nuclear and mitochondrial genomes to augment the ETC biogenesis that takes place in differentiating germ cells (Wang *et al*., 2019; Wang et al., 2023). Cytosolic and mitochondrial translation are up-regulated in concert to boost ETC biogenesis in budding yeast undergoing a metabolic shift from glycolysis to oxidative phosphorylation (Couvillion et al., 2016), further supporting the synchronized expression of ETC components from dual genetic origins at the translational level. Nevertheless, nuclear-encoded mitochondrial ETC subunits often exhibited a concordant expression pattern at the RNA level (Eisen et al., 1998), and mtDNA-encoded ETC RNAs consistently exhibited similar trends, albeit with a more gradual increase compared to their nuclear-encoded counterparts accompanying the metabolic shift (Couvillion *et al*., 2016). These observations suggest a potential coordination at the transcriptional level as well. We uncovered a

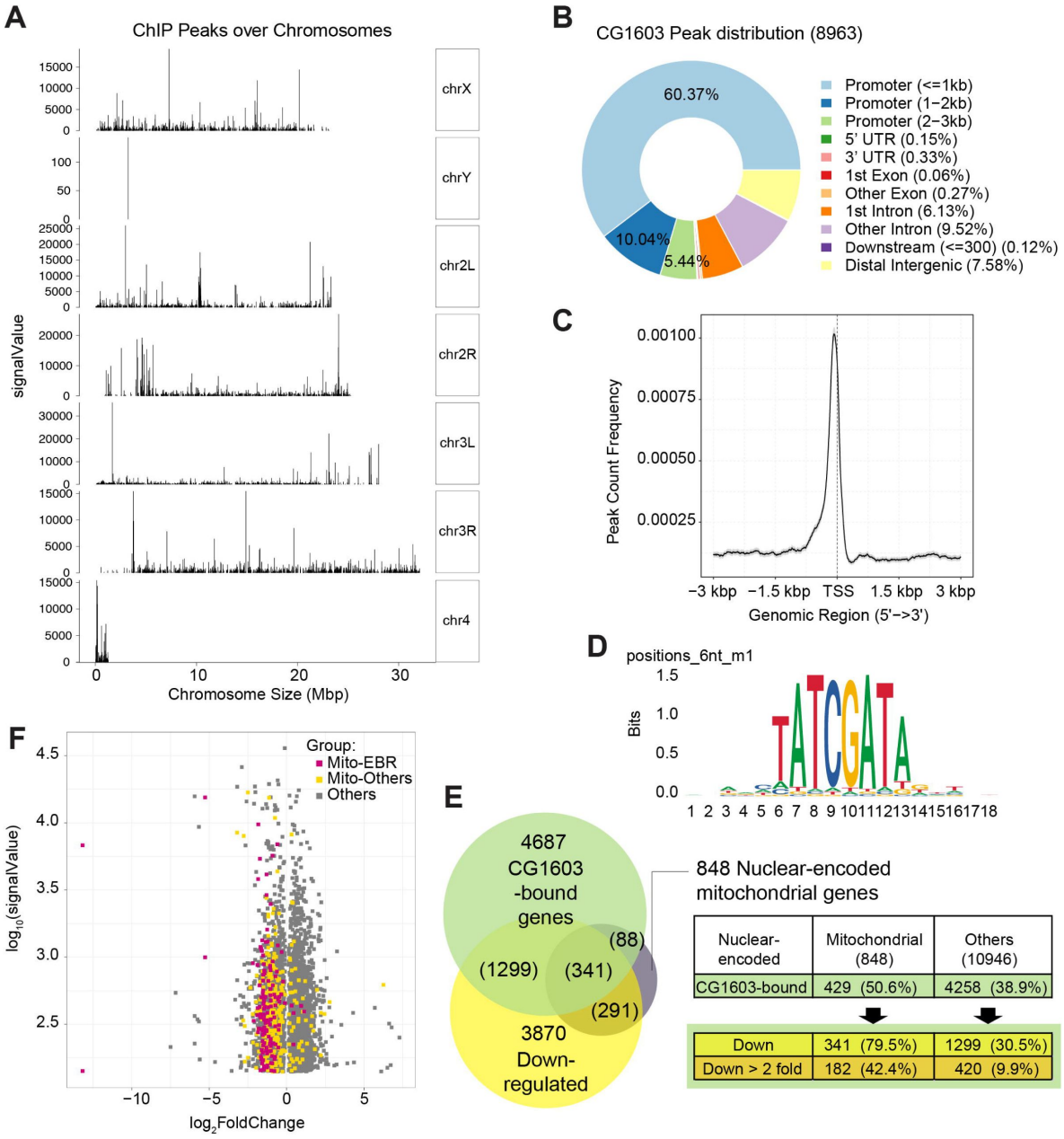

Figure 7.

ChIP analysis identified nuclear mitochondrial genes that may be directly regulated by CG1603.

(A) CG1603 ChIP peaks over all chromosomes. (B) Genomic distribution of CG1603 peaks. (C) Average profile of CG1603 peaks binding to transcription start site (TSS) regions. (D) Representative binding motif discovered with CG1603 ChIP peaks. (E) Summary of the number of nuclear-encoded mitochondrial and non-mitochondrial mRNA coding genes bound by CG1603, and the overlapping down-regulated differentially expressed genes (DEGs) in each group. (F) Scatterplot illustrating the signalValue of CG1603 ChIP peaks (y-axis) and log2 fold change in expression of DEGs between *CG1603*^{PBac} mutant and control (x-axis). MitoES: the genes belong to the categories that are clearly essential to mitochondrial ETC biogenesis and maintenance, including ETC subunits and assembly factors, mtDNA replication and transcription, mitochondrial RNA metabolism and translation, as well as mitochondrial protein import and membrane insertion machinery.

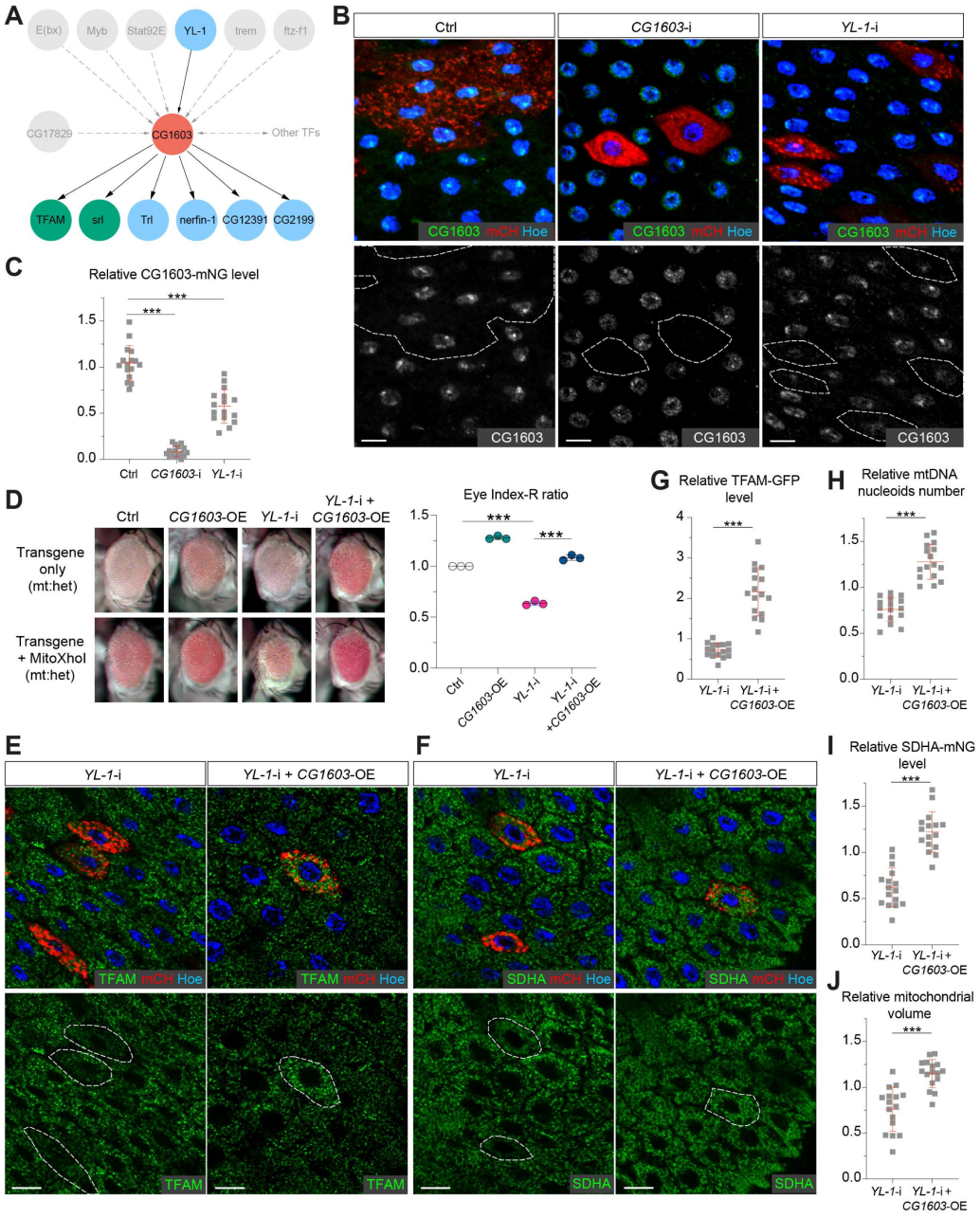

Figure 8.

YL-1 is an upstream regulator of CG1603.

(A) Schematic graph illustrating the CG1603 upstream and downstream (co-)TFs involved in regulating mitochondrial ETC biogenesis, inferred from ChIP-seq, RNAseq and genetics data. (B) Representative images of control RNAi (Ctrl), *CG1603* RNAi (*CG1603*-i) and *YL-1* RNAi (*YL-1*-i) midgut EC clones with endogenously expressed CG1603-mNG visualized in green or white. Clones were labeled by mCherry red and compared with wt neighbors. White dash lines aided in illustrating clones. Blue: Hoechst. Scale bars: 10 μm. (C) Quantification of the relative CG1603-mNG level in the EC clones to their wt neighbors. n=16 from 8 midguts for each group, error bar: SD. ***: p<0.001. (D) Representative eye image and Index-R ratio (RNAi + mitoXhoI / RNAi-only) of adult flies with indicated genotypes. Three biological repeats were performed for each group, error bar: SD. ***: p<0.001. (E-F) Representative images of *YL-1* RNAi (*YL-1*-i) and *YL-1* RNAi + *CG1603* overexpression (*YL-1*-i + *CG1603*-OE) midgut EC clones with endogenously expressed TFAM-GFP (E) or SDHA-mNG (F) visualized in green. Clones were labeled by mCherry red and compared with wt neighbors. Blue: Hoechst. Scale bars: 10 μm. (G-J) Quantification of the relative TFAM-GFP level (G), the relative mtDNA nucleoids number (H), the relative SDHA-mNG level (I) and the relative mitochondrial volume (J) in the EC clones to their wt neighbors. n=16 from 8 midguts for each group, error bar: SD. ***: p<0.001.

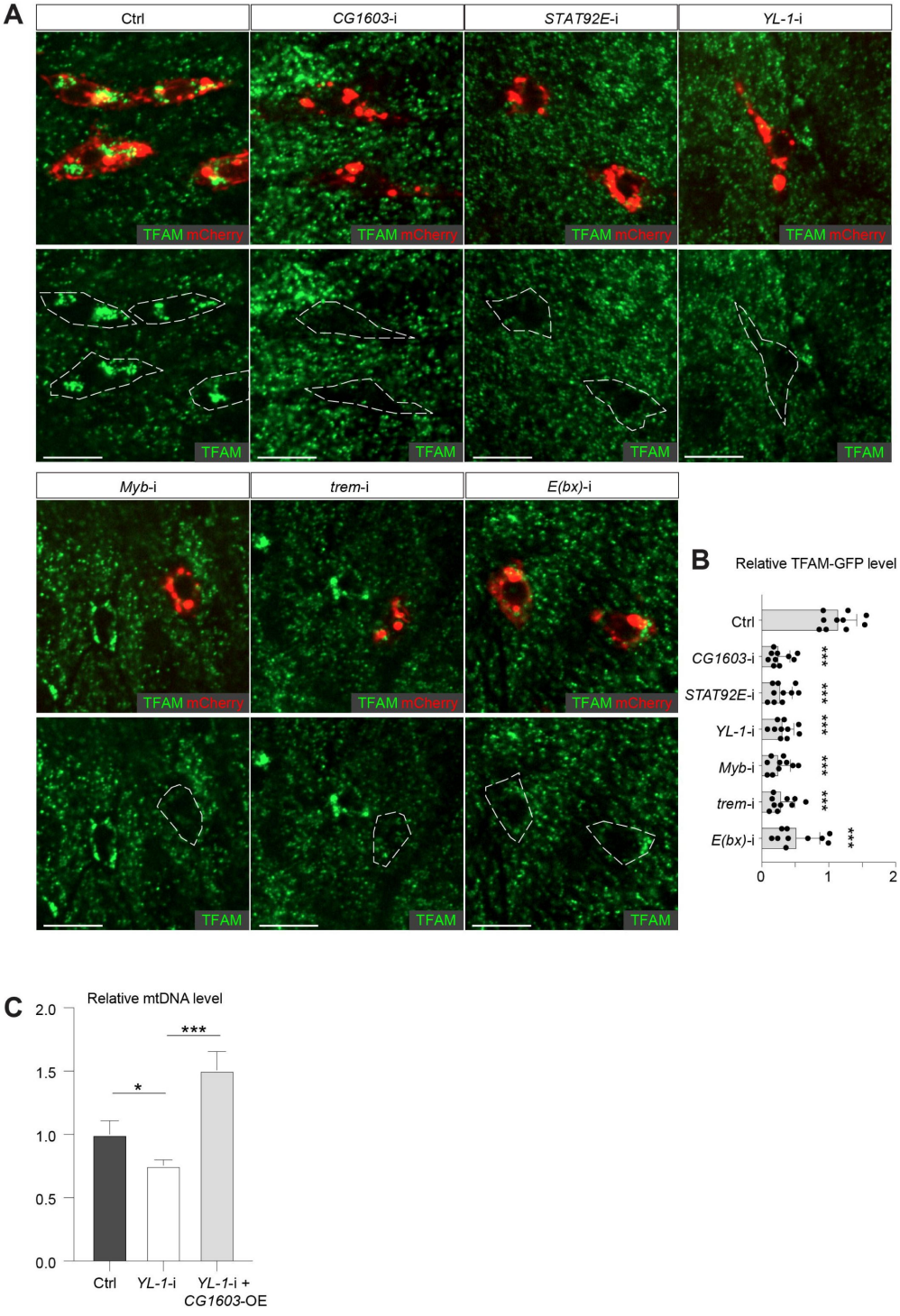

Figure 8-figure supplement

Figure 8—figure supplement A. Representative images of control RNAi (Ctrl), *CG1603* RNAi (*CG1603*-i), *STAT92E* RNAi (*STAT92E*-i), *YL-1* RNAi (*YL-1*-i), *Myb* RNAi (*Myb*-i), *trem* RNAi (*trem*-i) and *E(bx)* RNAi (*E(bx)*-i) midgut ISC/EB clones labeled by mCherry red, with endogenously expressed TFAM-GFP visualized in green. White dash lines aided in illustrating clones. Scale bars: 10 μm.
Figure 8—figure supplement B. Quantification of the relative TFAM-GFP level in midgut ISC/EB clones to their wt neighbors for different groups. n=10, error bar: SD. ***: p<0.001.
Figure 8—figure supplement C. Relative mtDNA levels in eye discs of different RNAi groups. n= 3, error bar: SD. *: P<0.05, ***: p<0.001.

zinc-finger protein encoded by the *CG1603* locus as a core regulator in a transcription network regulating mitochondrial biogenesis. CG1603 promoted the expression of more than half of nuclear-encoded mitochondrial proteins and the inhibition of CG1603 severely reduced mitochondrial mass and mtDNA contents. CG1603 targets were highly enriched in nuclear-encoded ETC subunits and essential factors required for mitochondrial DNA genome maintenance and gene expression. Thus, CG1603 not only promotes mitochondrial biogenesis in general, but also affords a transcriptional coordination of the nuclear and mitochondrial genomes in ETC biogenies.

The modifier screen in the developing eyes took advantage of the mtDNA deficiency resulted from the expression of MitoXhoI in a heteroplasmic background. Besides 77 enhancers, we also recovered 20 suppressors, of which "RNAi + MitoXhoI" flies had larger eyes than "RNAi-only" (**Figure 1G** and *Supplementary file 1*). Knockdown of these genes alone severely reduced eye size (**Figure 1G** and *Supplementary file 1*). Noteworthy, 5 of them were lethal due to the lack of head capsule that is developed from the eye antenna disc, but the viability of these RNAi flies was restored by MitoXhoI expression. Given that MitoXhoI expression also disrupts eye development, it is perplexing that the combination of RNAi and MitoXhoI expression, two genetic conditions causing the same phenotype, led to a milder phenotype. Perhaps, mitochondrial DNA deficiency caused by MitoXhoI expression triggers a retrograde signal, which boosts cellular stress responses and thereby mitigates the cell growth defects in these RNAi backgrounds.

The CG1603 belong to a large family of C2H2 Zinc finger (C2H2-ZF) transcription factors that contains 272 genes in *Drosophila* genome (*https://flybase.org/reports/FBgg0000732.html*). It has one N-terminus C2H2-ZF, followed by two MADFs and a cluster of six C2H2-ZFs at the C-terminus (**Figure 4A**). In addition to the C2H2-ZF cluster, which predominantly mediates sequence-specific DNA binding (Persikov et al., 2015; Wolfe et al., 2000), C2H2-ZF transcription factors often possess additional N-terminal protein-protein interaction domains, such as KRAB, SCAN and BTB/POZ domains in vertebrates, ZAD and BTB/POZ in *Drosophila*, for binding to transcription co-regulators (Fedotova et al., 2017; Perez-Torrado et al., 2006; Sobocinska et al., 2021). These interactions allow them to either activate or repress gene expression. CG1603 binds to the genomic regions of 4687 genes in the *Drosophila* genome. Among these genes, 602 and 562 genes were, respectively, decreased or increased more than two folds in *CG1603* mutant (*Supplementary file 6)*. Thus, CG1603 is likely a dual-function transcription factor, capable of both activating and repressing transcription depends on the chromosomal environment of its targets. Ying Yang 1, a well characterized dual-function transcription factor in mammals, contains both a transcription activation domain and a repression domain, in addition to four C2H2-ZFs at its C-terminus (Verheul et al., 2020). The N-terminus C2H2-ZF and the first MADF domain of CG1603 are negatively charged, thus have a low likelihood of binding to DNA that is also negatively charged (**Figure 4B**). In the predicted 3-D structure of CG1603, the positively charged C-terminal zinc fingers and MADF-2 domain cluster in the center, while the negatively charged N-terminal C2H2-ZF and the MADF-1 extend outward to the opposite directions (**Figure 4B**), resembling the domain arrangement of Ying Yang 1 (Verheul *et al*., 2020). MADF domains share significant similarity with Myb/SANT domains that may bind to either DNA or proteins (Maheshwari et al., 2008). Some MADF domains, due to their negative charge, have been proposed to interact with positively charged histone tails, similar to the Myb/SANT domain in a well-known chromatin remodeler ISWI, suggesting a potential role in chromatin remodeling (Maheshwari et al., 2008). Notably, some chromatin remodelers possess tandem Myb/SANT domains that can directly interact with histones and DNA or histone remodeling enzymes like ISWI and SMRT (Boyer et al., 2004). It is plausible that CG1603 may play a role in chromatin remodeling directly or by recruiting nucleosome remodeling factors to its binding sites, thereby modulating gene transcription in those regions. Notably, CG1603 had no impact on the expression of one third of its binding genes (*Supplementary file 6)*, highlighting that DNA binding profiling along is not sufficient to predict the function of a transcription factor. Nonetheless, the network analyses on TFs' ChIP-seq data allowed us to construct a potential regulatory network among these transcription factors, which

subsequently served as a blueprint for genetic analyses to verify potential regulations. Total 7 transcription factors were upstream of CG1603 in the network and emerged as positive hits in the initial screen in the eye. RNAi against 5 of them led to reduced TFAM level in the midgut, while the other two had no noticeable phenotype, suggesting that these two TFs may regulate mitochondrial biogenesis in a tissue specific manner. Only YL-1 was confirmed to act upstream of CG1603 based on the genetic epistasis analysis, further indicating the necessity of combining genomic, bioinformatic, and genetics analyses to gain more reliable and comprehensive understanding on transcriptional regulations. YL-1 is one of DNA binding subunits of the SRCAP complex, which is essential for histone H2A.Z incorporation and replacement (Liang *et al*., 2016). Recently, it has been shown that both SRCAP complex and H2A.Z are necessary for the transcription of nuclear-encoded mitochondrial genes (Lowden et al., 2021; Xu et al., 2021). Our work offers a mechanistic insight into how CG1603 and its upstream regulator, YL-1 may regulate mitochondrial biogenesis at nucleosome and chromatin level. Currently, most known transcription paradigms controlling mitochondrial biogenesis are centered on transcription factors and co-activators that stabilize or directly stimulate the core transcription machinery. The YL-1 to CG1603 cascade may represent a previously underappreciated layer of transcriptional regulation on ETC biogenesis and could act in concert with NRF1 and other transcription factors to coordinate both the nuclear and mitochondrial genome in ETC biogenesis.

Materials and methods

Fly genetics

Flies were maintained on standard cornmeal medium at 25°C, unless otherwise stated. Heteroplasmic lines that contain ~50% XhoI-resistant *mt:CoI*^{T300I} genome (Hill et al., 2014) were maintained at 18 °C. The heteroplasmic *w*^{1118}; *Sco / CyO, UAS-mitoXhoI; eyeless-GAL4* females were crossed with different RNAi lines to generate male offspring for assessing adult eye morphology. RNAi lines used in the screen were obtained from the Bloomington *Drosophila* Stock Center (BDSC), or Vienna *Drosophila* Resource Center, and listed in *Supplementary file 1*. *UAS-Luciferase* (BDSC#35788) was used as the transgene control. *TFAM-GFP* reporter line was described previously (Zhang *et al*., 2016). *Act>CD2>GAL4, UAS-mCD8::mCherry and hsFLP* (BDSC#7) were used to generated "flip-out" clones in midguts. We found that the leakage expression of flippase at 22°C was sufficient to induce "flip-out" clones. *PBac[SAstopDsRed]LL06826* (Kyoto#141919) was obtained from Kyoto Drosophila Stock Center, and backcrossed to *w*^{1118}for six generations before phenotypic analyses. A fluorescent "*CyO, act-GFP*" (BDSC#4533) was used for selecting homozygous mutant larvae. *PBac[SAstopDsRed]LL06826* was recombined with *FRT42D* (BDSC #1802) to generate *FRT42D, CG1603*^{PBac}, which was crossed with *hs-flp; FRT42D, Ubi-nls-RFP* (derived from BDSC#35496) for generating mitotic clones in ovaries (Laws and Drummond-Barbosa, 2015). Briefly, 0–2 days old females were transfer along with sibling males to the Kimwipe-semi-covered vials, then passed to 37°C water bath, heat shock for one hour, twice daily, for three consecutive days. The clones were assessed 7-10 days after the final heat shock. *Def*^{k08815}(BDSC#10818), *Def*^{Exel6052}(BDSC#7534) and *Def*^{Exel6053}(BDSC#7535) were obtained from BDSC.

Cell culture and Gene expression

S2 cells from Drosophila Genomics Resource Center (DGRC) were cultured as previously described (Zhang et al., 2015) following the online instruction (DRSC, *https://fgr.hms.harvard.edu/fly-cell-culture*). Briefly, cells were maintained in Schneider's medium (Thermo Fisher Scientific) with 10% heat inactivated Fetal Bovine Serum (FBS, Thermo Fisher Scientific) and 1% Penicillin-Streptomycin (Thermo Fisher Scientific) at 27 °C. Effectene Transfection Reagent (Qiagen) was used for plasmids transfection following manufacturer's instructions. For expression in S2 cells, the coding sequence of *CG1603* was cloned into a pIB vector (Thermo Fisher Scientific), with an *mCherry* coding sequence fused at the 3' end.

Transgenic flies

UASz-CG1603 plasmid was generated by inserting *CG1603* coding sequence between the Acc65I and XbaI sites of pUASz1.0 (*https://dgrc.bio.indiana.edu//stock/1431*; RRID: DGRC_1431). *UASz-CG1603* was inserted into either attP2 or attP40 (Bestgene Inc.) using PhiC31 integrase-mediated site-specific transformation, to generate transgenes on 3rd and 2nd chromosome, respectively.

The DNA fragment spanning *CG1603* genomic region was amplified by PCR and subcloned into a pattB vector (*https://dgrc.bio.indiana.edu//stock/1420*; RRID: DGRC_1420). The resulted plasmid was inserted into attP2 site (Bestgene Inc.) using PhiC31 integrase-mediated-specific transformation to generate the transgene *P[CG1603^{gDNA}]*.

SDHA-mNeonGreen reporter line was generated using a previous published method (Wang *et al.*, 2019). The targeting cassette comprising of 1 kb genomic DNA fragment upstream of *SDHA* stop codon, *mNeonGreen* coding sequence, a fragment containing *GMR-Hid* flanked by two FRT sites, and 1 kb genomic DNA fragment downstream of *SDHA* stop codon was inserted into a pENTR vector to make the homology donor construct. This donor construct and a *SDHA* chiRNA construct (*gRNA-SDHA* recognizes GTAGACATCCGTACGAGTGA[TGG]) were injected into the *Vasa-Cas9* expressing embryos (BDSC#51323). G0 adults were crossed with w1118 files, and progeny with small eye phenotype were selected as candidates due to the expression of *GMR-Hid*. To remove the *GMR-Hid* cassette, the *SDHA-mNeon-GMR-Hid* flies were crossed with *nos-Gal4; UASp-FLP*. The F1 progeny with the genotype of *nos-Gal4 / SDHA-mNeon-GMR-Hid; UASp-FLP / +* were selected and crossed with *Sco / CyO*. The F2 flies of *SDHA-mNeon / CyO* with normal white eyes were selected and maintained.

For *TFAM-mNeonGreen* and *CG1603-Halo-mNeonGreen* knock-In lines, the targeting cassette comprising of 1 kb genomic DNA fragment upstream of the stop codon, either *mNeonGreen* or *Halo-mNeonGreen* coding sequence, and 1 kb genomic DNA fragment downstream of the stop codon was inserted into pOT2 vector to generate the donor constructs. Each donor construct and the corresponding chiRNA construct (*gRNA for TFAM*: ATGATTTGTGAATTATGTGATGG; *gRNA for CG1603*: GGAATGAACTCTCGCCTTGAGGG) were injected into Vasa-Cas9 expressing embryos (BDSC#51323 or BDSC#51324). G0 adults were crossed with w1118 files, and the progeny carrying the *mNeonGreen* insertions were screened by PCR. Primers for TFAM-mNeonGreen are GCTCGCTGATCAACAAAGTC & GGTGGACTTCAGGTTTAACTCC. Primers for CG1603-mNeonGreen are AGTGCGAGTTCCTCAGT-GTG & CGCCCAGGACTTCCACATAA.

RNA sequencing analysis

For bulk RNA sequencing analysis, total RNA was extracted from wt and CG1603 mutant larvae (48h after egg laying) by Trizol (Thermo Fisher Scientific) following standard protocol. Three samples were used for each genotype. Poly (A) capture libraries were generated at the DNA Sequencing and Genomics Core, NHLBI, NIH. RNA sequencing was performed with using an Novaseq 6000 (Illumina) and 100-bp pair-end reads were generated at the DNA Sequencing and Genomics Core, NHLBI, NIH. Sequencing data were analyzed following the Bioinformatics Pipeline of mRNA Analysis, NCI, NIH. After quality assessment of FASTQ files using FastQC (*https://www.bioinformatics.babraham.ac.uk/projects/fastqc*), paired-end reads were aligned against Drosophila Melanogaster reference genome (Dmel6) using a two-pass method with STAR (v2.7.9a) (Dobin et al., 2013). Gene level read counts were produced by HTseq (v0.11.4) (Putri et al., 2022). Differential expression analysis at the gene-level was carried out using DESeq2 open-source R package (Love et al., 2014) with an FDR cut-off of 0.05. Gene Ontology (GO) enrichment analysis was performed by clusterProfiler R package (Yu et al., 2012) with the log2 fold change cut off >1 and < −1 for upregulated and down regulated genes, respectively. Density plot was

generated by ggplot2 R package (*https://ggplot2.tidyverse.org*). Drosophila mitochondrial genes and subgroups were referenced against a modified MitoCarta 3.0 inventory (Rath *et al*., 2021; Wang *et al*., 2019).

ChIP-seq computational analysis

ChIP-sequencing reads in FASTQ format and the narrowPeak output files for each candidate TF were downloaded from ENCODE Project open resource (*https://www.encodeproject.org*) (Kudron *et al*., 2018).

ChIP-sequencing reads were aligned to the Drosophila Melanogaster reference genome (Dmel6) using BWA (v0.7.17) (Li and Durbin, 2009). SAM files were sorted and compressed into BAM format with Samtools (v1.16.1) (Li et al., 2009). Replicates were merged by Picard tools (v2.27.3, *https://broadinstitute.github.io/picard*) using lenient criteria, and all alignments with a MAPQ value less than 20 were removed. Lags prediction and peak-calling were done with MACS2 (v2.2.7.1) (Zhang et al., 2008) following the ENCODE TF ChIP pipeline with IDR analysis performed for consistency analysis (*https://github.com/mforde84/ENCODE_TF_ChIP_pipeline*). Peak annotation and analysis of profile of ChIP peaks binding to TSS regions were performed with ChIPseeker R package (Yu et al., 2015). Transcription network was analyzed and visualized with VertexSort (Jothi *et al*., 2009) and igraph (*https://igraph.org*) R packages, respectively, and ChIP peaks of each TF identified in the gene promoter regions (<2kb) were used for analyses. CG1603 binding motif discovery was done by online integrated pipeline 'peak-motifs' of RSAT tools (*https://rsat.france-bioinformatique.fr/rsat/peak-motifs_form.cgi*) (Thomas-Chollier *et al*., 2012).

Imaging analyses

Imaging analyses were performed as previously described (Zhang *et al*., 2020) using the Zeiss Axio Observer equipped with a Perkin Elmer spinning disk confocal system or a Zeiss LSM880 confocal system. Tissues were dissected out and rinsed in room temperature Schneider's medium (Thermo Fisher Scientific) supplied with 10% heat inactivated fetal bovine serum (FBS; Thermo Fisher Scientific), and then used for either direct imaging or further staining and fixation. For live imaging, a Zeiss incubation system was used to maintain proper temperature, humidity. Live tissues were mounted with medium on the coverslip in a custom-made metal frame and then covered with a small piece of Saran wrap before imaging. For tissue fixation, PBS containing 4% PFA were used, followed by three times PBS washing. Hoechst 33342 and DAPI (5 μg/mL, Thermo Fisher Scientific) incubation in PBS for 5 min was used for nuclear staining of live tissues and fixed tissues, respectively. The image processing and quantification were performed by Volocity (Perkin Elmer, for image acquisition), Zen (Zeiss, for image acquisition), Imaris (Oxford Instruments, *https://imaris.oxinst.com/*, for 3D surface, voxels and intensity statistics) and Fiji / Image J software (NIH, *https://fiji.sc/*, for image processing and statistics) based on the previous published methods (Liu *et al*., 2022; Wang *et al*., 2023). The relative TFAM-GFP or TFAM -mNeonGreen level, or relative SDHA-mNeonGreen level was calculated as the ratio of the mean fluorescence intensity in the RNAi or mutant clone to that of its neighboring control, with background correction. The relative CG1603-mNG level was calculated as the ratio of the mean nuclear fluorescence intensity in the RNAi clone to that of its neighboring control, with background correction. The relative mtDNA nucleoids number was determined by calculating the ratio of the TFAM-GFP or TFAM -mNeonGreen puncta number in the RNAi or mutant clone, standardized by clone volume, to that of its neighboring control. The relative mitochondrial volume was calculated as the ratio of the total SDHA-GFP positive voxels with local contrast in the RNAi clone, standardized by clone volume, to that of its neighboring control.

Mitochondrial membrane potential was detected using a protocol adopted from a previously study (Zhang et al., 2020; Zhang et al., 2019). Briefly, after dissection, adult ovaries were incubated in the Schneider's medium containing TMRM (200nM, Thermo Fisher Scientific) and MitoTracker Green (200nM, Thermo Fisher Scientific) for 20 min at room temperature, rinsed with PBS for 3

times, and then imaged live within 1 h. TMRM and MitoTracker signal intensities were quantified and ratiometric image was generated using Fiji / Image J software (NIH). Mitochondrial membrane potential was computed as the ratio of the mean intensity of TMRM to MitoTracker fluorescence with background correction.

Western blot

Protein extracts from wt and *CG1603* mutant larvae tissues (48h after egg laying) were prepared using the RIPA buffer (MilliporeSigma) with Halt Protease Inhibitor Cocktail (Thermo Fisher Scientific), 5 mM NaF (MilliporeSigma) and 1 mM Na3VO4 (MilliporeSigma). Western blot was performed using a XCell SureLock™ Mini-Cell and XCell II™ Blot Module (Thermo Fisher Scientific). Samples were electrophoresed under a reducing condition on NuPAGE™ 4 to 12% Bis-Tris Mini Protein Gels (Thermo Fisher Scientific). Proteins on the gel were transferred to a Polyvinylidene Difluoride (PVDF) membrane (Thermo Fisher Scientific). The membranes were blocked with 5% BSA or non-fat milk (MilliporeSigma) in TBST (Tris buffered saline with 0.1% Tween-20). After a serial of washes and incubations with primary antibodies, TBST and secondary antibodies, the immunoreactivity was visualized using SuperSignal West Dura Chemiluminescent Substrate (Thermo Fisher Scientific) and Amersham ImageQuant 800 system (Cytiva). The antibodies used were: Mouse anti-Actin antibody (C4, MilliporeSigma), Mouse anti-ATP5A antibody (15H4C4, abcam), Mouse anti-ND30 antibody (17D95, abcam), rabbit anti-TFAM antibody (Liu *et al*., 2022), rabbit anti-HSP60 antibody (#4870, Cell Signaling), Anti-rabbit IgG, HRP-linked Antibody (#7074, Cell Signaling) and Anti-mouse IgG, HRP-linked Antibody (#7076, Cell Signaling).

Blue native PAGE and in-gel activity assays of ETC complexes

Mitochondria from fly larvae were isolated by homogenization and differential centrifugation following previous protocol (Chen et al., 2015). Solubilized protein samples from isolated mitochondria were prepared with NativePAGE™ Sample Prep Kit (Thermo Fisher Scientific) and the concentrations were determined by Pierce BCA protein assay (Thermo Fisher Scientific). Blue native PAGE was performed using NativePAGE™ 4–16% Bis-Tris gels and NativePAGE™ Running Buffer Kit (Thermo Fisher Scientific) according to the manufacturer's protocol. 60 µg proteins each sample were used. For in-gel activity assays, gels were incubated with one of the following solutions: Complex I buffer (5mM Tris-HCl pH 7.4; 0.1mg/ml NADH; 2.5mg/ml Nitro Blue Tetrazolium), Complex II buffer (5mM Tris-HCl pH 7.4; 20mM sodium succinate; 0.2mM phenazine methasulfate; 2.5mg/ml Nitro Blue Tetrazolium) or Complex IV buffer (50mM sodium phosphate pH 7.2; 0.05% 3,3'-diaminobenzidine tetrahydrochloride, 50µM horse heart cytochrome c) at room temperature for hours, stopped by fixation with 50% methanol and 10% acetic acid for 30 min and washed with 10% acetic acid. All chemicals from MilliporeSigma.

Quantitative real-time PCR

Total genomic DNAs or RNAs were isolated using the DNeasy Blood & Tissue Kit (Qiagen) and RNeasy Mini Kit (Qiagen), respectively, following the manufacturers' instructions. cDNAs were synthesized by the SuperScript VILO cDNA Synthesis Kit (Thermo Fisher Scientific). Real-time PCRs were performed in triplicate using the PowerTrack SYBR Green Master Mix (Thermo Fisher Scientific), MicroAmp™Optical 96-Well Reaction Plate with Barcode (Thermo Fisher Scientific), and QuantStudio™ 3 Real-Time PCR System (Thermo Fisher Scientific). Primers for amplifying mtDNA and nuclear DNA (nuDNA), as well as for measuring gene expression levels are listed in *Supplementary file 8*. The relative mtDNA levels of fly larvae or eye discs were measured in three biological replicates for each group using total DNAs extractedfrom twenty larvae or eye discs. The relative mRNA levels of ETC genes were measured in three biological replicates for each group using total RNAs extracted from twenty larvae.

Prediction of protein domains, isoelectric point (pI), net charge and structure

Protein domains were predicted via SMART (Schultz et al., 2000). Protein domain pI and net charge were predicted using bioinformatic toolbox, Prot pi (*https://www.protpi.ch/Calculator/ProteinTool*). Protein 3D structure was predicted by AlphaFold (Jumper et al., 2021).

Statistical analysis

Two-tailed Student's t-test was used for statistical analysis. Difference was considered statistically significant when $P<0.05$. Results are represented as mean ± SD of the number of determinations.

Acknowledgements

We thank Bloomington Drosophila Stock Center, Vienna Drosophila Resource Center and Kyoto Drosophila Genomics and Genetics Resources for various fly lines; NHLBI Light Microscope Core and NHLBI DNA Sequencing and Genomics Core for technical assistance. This work is supported by NHLBI Intramural Research Program.

References

Acosta-Alvear D., Zhou Y., Blais A., Tsikitis M., Lents N.H., Arias C., Lennon C.J., Kluger Y., Dynlacht B.D (2007) **XBP1 controls diverse cell type- and condition-specific transcriptional regulatory networks** *Mol Cell* **27**:53–66 https://doi.org/10.1016/j.molcel.2007.06.011

Alam T.I., Kanki T., Muta T., Ukaji K., Abe Y., Nakayama H., Takio K., Hamasaki N., Kang D (2003) **Human mitochondrial DNA is packaged with TFAM** *Nucleic Acids Res* **31**:1640–1645 https://doi.org/10.1093/nar/gkg251

Angelini C., Costa V (2014) **Understanding gene regulatory mechanisms by integrating ChIP-seq and RNA-seq data: statistical solutions to biological problems** *Front Cell Dev Biol* **2** https://doi.org/10.3389/fcell.2014.00051

Berger J., Moller D.E (2002) **The mechanisms of action of PPARs** *Annu Rev Med* **53**:409–435 https://doi.org/10.1146/annurev.med.53.082901.104018

Boyer L.A., Latek R.R., Peterson C.L (2004) **The SANT domain: a unique histone-tail-binding module?** *Nat Rev Mol Cell Biol* **5**:158–163 https://doi.org/10.1038/nrm1314

Chen Z., Qi Y., French S., Zhang G., Covian Garcia R., Balaban R., Xu H (2015) **Genetic mosaic analysis of a deleterious mitochondrial DNA mutation in Drosophila reveals novel aspects of mitochondrial regulation and function** *Mol Biol Cell* **26**:674–684 https://doi.org/10.1091/mbc.E14-11-1513

Chen Z., Wang Z.H., Zhang G., Bleck C.K.E., Chung D.J., Madison G.P., Lindberg E., Combs C., Balaban R.S., Xu H (2020) **Mitochondrial DNA segregation and replication restrict the transmission of detrimental mutation** *J Cell Biol* **219** https://doi.org/10.1083/jcb.201905160

Chen Z., Zhang F., Xu H (2019) **Human mitochondrial DNA diseases and Drosophila models** *J Genet Genomics* **46**:201–212 https://doi.org/10.1016/j.jgg.2019.03.009

Couvillion M.T., Soto I.C., Shipkovenska G., Churchman L.S (2016) **Synchronized mitochondrial and cytosolic translation programs** *Nature* **533**:499–503 https://doi.org/10.1038/nature18015

Deblois G., Giguere V (2011) **Functional and physiological genomics of estrogen-related receptors (ERRs) in health and disease** *Biochim Biophys Acta* **1812**:1032–1040 https://doi.org/10.1016/j.bbadis.2010.12.009

Dobin A., Davis C.A., Schlesinger F., Drenkow J., Zaleski C., Jha S., Batut P., Chaisson M., Gingeras T.R (2013) **STAR: ultrafast universal RNA-seq aligner** *Bioinformatics* **29**:15–21 https://doi.org/10.1093/bioinformatics/bts635

Eisen M.B., Spellman P.T., Brown P.O., Botstein D (1998) **Cluster analysis and display of genome-wide expression patterns** *Proc Natl Acad Sci U S A* **95**:14863–14868 https://doi.org/10.1073/pnas.95.25.14863

Falkenberg M., Gaspari M., Rantanen A., Trifunovic A., Larsson N.G., Gustafsson C.M (2002) **Mitochondrial transcription factors B1 and B2 activate transcription of human mtDNA** *Nature genetics* **31**:289–294 https://doi.org/10.1038/ng909

Fedotova A.A., Bonchuk A.N., Mogila V.A., Georgiev P.G. (2017) **C2H2 Zinc Finger Proteins: The Largest but Poorly Explored Family of Higher Eukaryotic Transcription Factors** *Acta Naturae* **9**:47–58

Fernandez-Vizarra E., Enriquez J.A., Perez-Martos A., Montoya J., Fernandez-Silva P (2011) **Tissue-specific differences in mitochondrial activity and biogenesis** *Mitochondrion* **11**:207–213 https://doi.org/10.1016/j.mito.2010.09.011

Finck B.N., Kelly D.P. (2007) **Peroxisome proliferator-activated receptor gamma coactivator-1 (PGC-1) regulatory cascade in cardiac physiology and disease** *Circulation* **115**:2540–2548 https://doi.org/10.1161/CIRCULATIONAHA.107.670588

Gorman G.S., Chinnery P.F., DiMauro S., Hirano M., Koga Y., McFarland R., Suomalainen A., Thorburn D.R., Zeviani M., Turnbull D.M (2016) **Mitochondrial diseases** *Nat Rev Dis Primers* **2** https://doi.org/10.1038/nrdp.2016.80

Hill J.H., Chen Z., Xu H. (2014) **Selective propagation of functional mitochondrial DNA during oogenesis restricts the transmission of a deleterious mitochondrial variant** *Nature genetics* **46**:389–392 https://doi.org/10.1038/ng.2920

Hock M.B., Kralli A (2009) **Transcriptional control of mitochondrial biogenesis and function** *Annu Rev Physiol* **71**:177–203 https://doi.org/10.1146/annurev.physiol.010908.163119

Jiang S., Mortazavi A (2018) **Integrating ChIP-seq with other functional genomics data** *Brief Funct Genomics* **17**:104–115 https://doi.org/10.1093/bfgp/ely002

Jothi R., Balaji S., Wuster A., Grochow J.A., Gsponer J., Przytycka T.M., Aravind L., Babu M.M (2009) **Genomic analysis reveals a tight link between transcription factor dynamics and regulatory network architecture** *Mol Syst Biol* **5** https://doi.org/10.1038/msb.2009.52

Jumper J. *et al.* (2021) **Highly accurate protein structure prediction with AlphaFold** *Nature* **596**:583–589 https://doi.org/10.1038/s41586-021-03819-2

Kudron M.M. *et al.* (2018) **The ModERN Resource: Genome-Wide Binding Profiles for Hundreds of Drosophila and Caenorhabditis elegans Transcription Factors** *Genetics* **208**:937–949 https://doi.org/10.1534/genetics.117.300657

Kurland C.G., Andersson S.G (2000) **Origin and evolution of the mitochondrial proteome** *Microbiol Mol Biol Rev* **64**:786–820 https://doi.org/10.1128/MMBR.64.4.786-820.2000

Laws K.M., Drummond-Barbosa D (2015) **Genetic Mosaic Analysis of Stem Cell Lineages in the Drosophila Ovary** *Methods Mol Biol* **1328**:57–72 https://doi.org/10.1007/978-1-4939-2851-4_4

Li H., Durbin R (2009) **Fast and accurate short read alignment with Burrows-Wheeler transform** *Bioinformatics* **25**:1754–1760 https://doi.org/10.1093/bioinformatics/btp324

Li H., Handsaker B., Wysoker A., Fennell T., Ruan J., Homer N., Marth G., Abecasis G., Durbin R., Genome Project Data Processing, S. (2009) **The Sequence Alignment/Map format and SAMtools** *Bioinformatics* **25**:2078–2079 https://doi.org/10.1093/bioinformatics/btp352

Liang X. *et al.* (2016) **Structural basis of H2A.Z recognition by SRCAP chromatin-remodeling subunit YL1** *Nat Struct Mol Biol* **23**:317–323 https://doi.org/10.1038/nsmb.3190

Liao T.S. *et al.* (2006) **An efficient genetic screen in Drosophila to identify nuclear-encoded genes with mitochondrial function** *Genetics* **174**:525–533 https://doi.org/10.1534/genetics.106.061705

Liu Y., Chen Z., Wang Z.H., Delaney K.M., Tang J., Pirooznia M., Lee D.Y., Tunc I., Li Y., Xu H (2022) **The PPR domain of mitochondrial RNA polymerase is an exoribonuclease required for mtDNA replication in Drosophila melanogaster** *Nat Cell Biol* **24**:757–765 https://doi.org/10.1038/s41556-022-00887-y

Love M.I., Huber W., Anders S (2014) **Moderated estimation of fold change and dispersion for RNA-seq data with DESeq2** *Genome Biol* **15** https://doi.org/10.1186/s13059-014-0550-8

Lowden C. *et al.* (2021) **Homeostatic control of nuclear-encoded mitochondrial gene expression by the histone variant H2A.Z is essential for neuronal survival** *Cell Rep* **36** https://doi.org/10.1016/j.celrep.2021.109704

Maheshwari S., Wang J., Barbash D.A (2008) **Recurrent positive selection of the Drosophila hybrid incompatibility gene Hmr** *Mol Biol Evol* **25**:2421–2430 https://doi.org/10.1093/molbev/msn190

Mandal S., Guptan P., Owusu-Ansah E., Banerjee U (2005) **Mitochondrial regulation of cell cycle progression during development as revealed by the tenured mutation in Drosophila** *Dev Cell* **9**:843–854 https://doi.org/10.1016/j.devcel.2005.11.006

Owusu-Ansah E., Yavari A., Mandal S., Banerjee U (2008) **Distinct mitochondrial retrograde signals control the G1-S cell cycle checkpoint** *Nature genetics* **40**:356–361 https://doi.org/10.1038/ng.2007.50

Park P.J (2009) **ChIP-seq: advantages and challenges of a maturing technology** *Nat Rev Genet* **10**:669–680 https://doi.org/10.1038/nrg2641

Perez-Torrado R., Yamada D., Defossez P.A (2006) **Born to bind: the BTB protein-protein interaction domain** *Bioessays* **28**:1194–1202 https://doi.org/10.1002/bies.20500

Persikov A.V., Wetzel J.L., Rowland E.F., Oakes B.L., Xu D.J., Singh M., Noyes M.B (2015) **A systematic survey of the Cys2His2 zinc finger DNA-binding landscape** *Nucleic Acids Res* **43**:1965–1984 https://doi.org/10.1093/nar/gku1395

Prober D.A., Edgar B.A. (2000) **Ras1 promotes cellular growth in the Drosophila wing** *Cell* **100**:435–446 https://doi.org/10.1016/s0092-8674(00)80679-0

Putri G.H., Anders S., Pyl P.T., Pimanda J.E., Zanini F (2022) **Analysing high-throughput sequencing data in Python with HTSeq 2.0** *Bioinformatics* https://doi.org/10.1093/bioinformatics/btac166

Rath S. *et al.* (2021) **MitoCarta3.0: an updated mitochondrial proteome now with sub-organelle localization and pathway annotations** *Nucleic Acids Res* **49**:D1541–D1547 https://doi.org/10.1093/nar/gkaa1011

Rouyer F., Rachidi M., Pikielny C., Rosbash M (1997) **A new gene encoding a putative transcription factor regulated by the Drosophila circadian clock** *EMBO J* **16**:3944–3954 https://doi.org/10.1093/emboj/16.13.3944

Scarpulla R.C (2008) **Transcriptional paradigms in mammalian mitochondrial biogenesis and function** *Physiol Rev* **88**:611–638 https://doi.org/10.1152/physrev.00025.2007

Scarpulla R.C., Vega R.B., Kelly D.P (2012) **Transcriptional integration of mitochondrial biogenesis** *Trends Endocrinol Metab* **23**:459–466 https://doi.org/10.1016/j.tem.2012.06.006

Schuldiner O., Berdnik D., Levy J.M., Wu J.S., Luginbuhl D., Gontang A.C., Luo L (2008) **piggyBac-based mosaic screen identifies a postmitotic function for cohesin in regulating developmental axon pruning** *Dev Cell* **14**:227–238 https://doi.org/10.1016/j.devcel.2007.11.001

Schultz J., Copley R.R., Doerks T., Ponting C.P., Bork P (2000) **SMART: a web-based tool for the study of genetically mobile domains** *Nucleic Acids Res* **28**:231–234 https://doi.org/10.1093/nar/28.1.231

Shen K., Pender C.L., Bar-Ziv R., Zhang H., Wickham K., Willey E., Durieux J., Ahmad Q., Dillin A (2022) **Mitochondria as Cellular and Organismal Signaling Hubs** *Annu Rev Cell Dev Biol* **38**:179–218 https://doi.org/10.1146/annurev-cellbio-120420-015303

Sobocinska J., Molenda S., Machnik M., Oleksiewicz U (2021) **KRAB-ZFP Transcriptional Regulators Acting as Oncogenes and Tumor Suppressors: An Overview** *Int J Mol Sci* **22** https://doi.org/10.3390/ijms22042212

Spinelli J.B., Haigis M.C (2018) **The multifaceted contributions of mitochondria to cellular metabolism** *Nat Cell Biol* **20**:745–754 https://doi.org/10.1038/s41556-018-0124-1

Taylor R.W., Turnbull D.M (2005) **Mitochondrial DNA mutations in human disease** *Nat Rev Genet* **6**:389–402 https://doi.org/10.1038/nrg1606

Thomas-Chollier M., Darbo E., Herrmann C., Defrance M., Thieffry D., van Helden J. (2012) **A complete workflow for the analysis of full-size ChIP-seq (and similar) data sets using peak-motifs** *Nat Protoc* **7**:1551–1568 https://doi.org/10.1038/nprot.2012.088

Verheul T.C.J., van Hijfte L., Perenthaler E., Barakat T.S. (2020) **The Why of YY1: Mechanisms of Transcriptional Regulation by Yin Yang 1** *Front Cell Dev Biol* **8** https://doi.org/10.3389/fcell.2020.592164

Wang Z.H., Liu Y., Chaitankar V., Pirooznia M., Xu H (2019) **Electron transport chain biogenesis activated by a JNK-insulin-Myc relay primes mitochondrial inheritance in Drosophila** *Elife* **8** https://doi.org/10.7554/eLife.49309

Wang Z.H., Zhao W., Combs C.A., Zhang F., Knutson J.R., Lilly M.A., Xu H (2023) **Mechanical stimulation from the surrounding tissue activates mitochondrial energy metabolism in Drosophila differentiating germ cells** *Dev Cell* https://doi.org/10.1016/j.devcel.2023.08.007

Wiedemann N., Pfanner N (2017) **Mitochondrial Machineries for Protein Import and Assembly** *Annu Rev Biochem* **86**:685–714 https://doi.org/10.1146/annurev-biochem-060815-014352

Wolfe S.A., Nekludova L., Pabo C.O (2000) **DNA recognition by Cys2His2 zinc finger proteins** *Annu Rev Biophys Biomol Struct* **29**:183–212 https://doi.org/10.1146/annurev.biophys.29.1.183

Wysocka J. *et al.* (2006) **A PHD finger of NURF couples histone H3 lysine 4 trimethylation with chromatin remodelling** *Nature* **442**:86–90 https://doi.org/10.1038/nature04815

Xu H., DeLuca S.Z., O'Farrell P.H (2008) **Manipulating the metazoan mitochondrial genome with targeted restriction enzymes** *Science* **321**:575–577 https://doi.org/10.1126/science.1160226

Xu M., Yao J., Shi Y., Yi H., Zhao W., Lin X., Yang Z (2021) **The SRCAP chromatin remodeling complex promotes oxidative metabolism during prenatal heart development** *Development* **148** https://doi.org/10.1242/dev.199026

Yu G., Wang L.G., Han Y., He Q.Y (2012) **clusterProfiler: an R package for comparing biological themes among gene clusters** *Omics* **16**:284–287 https://doi.org/10.1089/omi.2011.0118

Yu G., Wang L.G., He Q.Y (2015) **ChIPseeker: an R/Bioconductor package for ChIP peak annotation, comparison and visualization** *Bioinformatics* **31**:2382–2383 https://doi.org/10.1093/bioinformatics/btv145

Zhang F., Pirooznia M., Xu H (2020) **Mitochondria regulate intestinal stem cell proliferation and epithelial homeostasis through FOXO** *Mol Biol Cell* **31**:1538–1549 https://doi.org/10.1091/mbc.E19-10-0560

Zhang F., Qi Y., Zhou K., Zhang G., Linask K., Xu H (2015) **The cAMP phosphodiesterase Prune localizes to the mitochondrial matrix and promotes mtDNA replication by stabilizing TFAM** *EMBO Rep* **16**:520–527 https://doi.org/10.15252/embr.201439636

Zhang Y., Chen Y., Gucek M., Xu H (2016) **The mitochondrial outer membrane protein MDI promotes local protein synthesis and mtDNA replication** *EMBO J* **35**:1045–1057 https://doi.org/10.15252/embj.201592994

Zhang Y. *et al.* (2008) **Model-based analysis of ChIP-Seq (MACS)** *Genome Biol* **9** https://doi.org/10.1186/gb-2008-9-9-r137

Zhang Y., Wang Z.H., Liu Y., Chen Y., Sun N., Gucek M., Zhang F., Xu H (2019) **PINK1 Inhibits Local Protein Synthesis to Limit Transmission of Deleterious Mitochondrial DNA Mutations** *Mol Cell* **73**:1127–1137 https://doi.org/10.1016/j.molcel.2019.01.013

Zhou W., Sherwood B., Ji H (2016) **Computational Prediction of the Global Functional Genomic Landscape: Applications, Methods, and Challenges** *Hum Hered* **81**:88–105 https://doi.org/10.1159/000450827

Author information

Fan Zhang

National Heart, Lung, and Blood Institute, National Institutes of Health, Bethesda, USA

Annie Lee
National Heart, Lung, and Blood Institute, National Institutes of Health, Bethesda, USA

Anna Freitas
National Heart, Lung, and Blood Institute, National Institutes of Health, Bethesda, USA

Jake Herb
National Heart, Lung, and Blood Institute, National Institutes of Health, Bethesda, USA

Zongheng Wang
National Heart, Lung, and Blood Institute, National Institutes of Health, Bethesda, USA

Snigdha Gupta
National Heart, Lung, and Blood Institute, National Institutes of Health, Bethesda, USA

Zhe Chen
National Heart, Lung, and Blood Institute, National Institutes of Health, Bethesda, USA

Hong Xu
National Heart, Lung, and Blood Institute, National Institutes of Health, Bethesda, USA
ORCID iD: 0000-0002-1423-1809

For correspondence: Hong.Xu@nih.gov

Editors

Reviewing Editor
Hugo Bellen
Baylor College of Medicine, Houston, United States of America

Senior Editor
Benoit Kornmann
University of Oxford, Oxford, United Kingdom

Reviewer #1 (Public review):

In this manuscript, Zhang et al. report a genetic screen to identify novel transcriptional regulators that coordinate mitochondrial biogenesis. They performed an RNAi-based modifier screen wherein they systematically knocked down all known transcription factors in the developing Drosophila eye, which was sensitized and had decreased mitochondrial DNA content. Through this screen, they identify CG1603 as a potential regulator of mitochondrial volume. They show that protein levels of mitochondrial proteins like TFAM, SDHA, and other mitochondrial proteins and mtDNA content are downregulated in CG1603 mutants. RNA-Seq and ChIP-Seq further show that CG1603 binds to the promoter regions of several known nuclear-encoded mitochondrial genes and regulates their expression. Finally, they also identified YL-1 as an upstream regulator of CG1603. Most studies have focused on PGC-1α as a master regulator of mitochondrial biogenesis. which seems to be a context-dependent regulator. Also, PGC-1α mediated regulation does not explain the regulation of 1100 genes that are required for mitochondrial biogenesis. Therefore, identifying new regulators in this work is crucial for the advancement of our understanding of mitochondrial biogenesis.

https://doi.org/10.7554/eLife.96536.2.sa2

Reviewer #2 (Public review):

Summary:

In this study, the authors identified nuclear genome-encoded transcription factors that regulate mtDNA maintenance and mitochondrial biogenesis. They started with an RNAi screening in developing Drosophila eyes with reduced mtDNA content and identified several putative candidate genes. Subsequently, using ChIP-seq data, they built a potential regulatory network that seems to govern mitochondrial biogenesis. Next, they focused on a candidate gene, CG1603 /clifford, for further characterization. Based on the expression of different markers, such as TFAM and SDHA, in RNAi and overexpression clones in the midgut, they argued that CG1603 promotes mitochondrial biogenesis and the expression of ETC complex genes. They used a CG1603 mutant to show reduced mtDNA and mitochondrial protein levels. Clonal analyses showed a reduction in mitochondrial biogenesis and membrane potential upon loss of CG1603. They further showed that the protein is localized to the mitochondria, and binds to polytene chromosomes in the salivary gland. Based on the RNA-seq results from the mutants and the ChIP data, the authors argued that the nucleus-encoded mitochondrial genes are downregulated >2 folds in the CG1603 mutants and that the regulatory elements bound by CG1603 are related to ETC biogenesis. Finally, they showed that YL-1, another candidate in the network, is an upstream regulator of CG1603. The screening strategy was well-designed, and the follow-up experiments were nicely executed.

Comments on revisions:

The authors have addressed my previous comments satisfactorily.

https://doi.org/10.7554/eLife.96536.2.sa1

Author response:

The following is the authors' response to the original reviews.

> ***Public Reviews:***
>
> ***Reviewer #1 (Public Review):***
>
> *Summary:*
>
> *In this manuscript, Zhang et al. report a genetic screen to identify novel transcriptional regulators that could coordinate mitochondrial biogenesis. They performed an RNAi-based modifier screen wherein they systematically knocked down all known transcription factors in the developing Drosophila eye, which was already sensitised and had decreased mitochondrial DNA content. Through this screen, they identify CG1603 as a potential regulator of mitochondrial content. They show that protein levels of mitochondrial proteins like TFAM, SDHA, and other mitochondrial proteins and mtDNA content are downregulated in CG1603 mutants. RNA-Seq and ChIP-Seq further show that CG1603 binds to the promoter regions of several known nuclear-encoded mitochondrial genes and regulates their expression. Finally, they also identified YL-1 as an upstream regulator of CG1603. Overall, it is a very important study as our understanding of the regulation of mitochondrial biogenesis remains limited across metazoans. Most studies have focused on PGC-1α as a master regulator of mitochondrial biogeneis, which seems a context-dependent regulator. Also, PGC-1α mediated regulation could not explain the regulation of 1100 genes that are required for mitochondrial biogenesis. Therefore,*

identifying a new regulator is crucial for understanding the overall regulation of mitochondrial biogenesis.

Reviewer #2 (Public Review):

Summary:

In this study, the authors aim to identify the nuclear genome-encoded transcription factors that regulate mtDNA maintenance and mitochondrial biogenesis. They started with an RNAi screening in developing Drosophila eyes with reduced mtDNA content and identified a number of putative candidate genes. Subsequently, using ChIP-seq data, they built a potential regulatory network that could govern mitochondrial biogenesis. Next, they focused on a candidate gene, CG1603, for further characterization. Based on the expression of different markers, such as TFAM and SDHA, in the RNAi and OE clones in the midgut cells, they argue that CG1603 promotes mitochondrial biogenesis and the expression of ETC complex genes. Then, they used a mutant of CG1603 and showed that both mtDNA levels and mitochondrial protein levels were reduced. Using clonal analyses, they further show a reduction in mitochondrial biogenesis and membrane potential upon loss of CG1603. They made a reporter line of CG1603, showed that the protein is localized to the mitochondria, and binds to polytene chromosomes in the salivary gland. Based on the RNA-seq results from the mutants and the ChIP data, the authors argue that the nucleus-encoded mitochondrial genes that are downregulated >2 folds in the CG1603 mutants and that are bound by CG1603 are related to ETC biogenesis. Finally, they show that YL-1, another candidate in the network, is an upstream regulator of CG1603.

Strengths:

This is a valuable study, which identifies a potential regulator and a network of nucleus-encoded transcription factors that regulate mitochondrial biogenesis. Through in-vivo and in-vitro experimental evidence, the authors identify the role of CG1603 in this process. The screening strategy was smart, and the follow-up experiments were nicely executed.

Weaknesses:

Some additional experiments showing the effects of CG1603 loss on ETC integrity and functionality would strengthen the work.

Recommendations for the authors:

Reviewer #1 (Recommendations For The Authors):

(1) Fig 3F: SDHA levels are severely downregulated in CG1603 RNAi clones. Therefore, estimating mitochondrial volume based on the SDHA reporter might be misleading. I suggest the authors perform this experiment with an independent marker of mitochondria, like mitoTracker Green or other dyes. I also suggest checking for mitochondrial number/quantity/size by electron microscopy.

Even though being downregulated, the SDHA-mNeon signal in EC clones clearly outlined mitochondria and the overall mitochondrial network, allowing us to quantify the total mitochondrial volume. Examining mitochondrial number/quantity/size by electron microscopy would further strengthen this statement, and we will consider it in future studies.

(2) The authors might comment on whether there was any decrease in the volume of CG1603i clone cells. And whether this was taken into account while normalising the mitochondrial volume.

The size/volume of CG1603i clone cells were indeed decreased, which was considered while normalizing the mitochondrial volume. We clarified this point in methods section (page 18, line 511-512 (revised version page 18, line 515-517)).

> *(3) Line 230-234: Collectively, these results demonstrate that CG1603 promotes the expression of both nuclear and mtDNA-encoded ETC genes and boosts mitochondrial biogenesis. CG1603 RNAi produced very few EC clones, consistent with the notion that mitochondrial respiration is necessary for ISCs differentiation.*
>
> *(4) Quantifying the number of EC clone cells observed might help support this statement.*

This is a great point. We quantified the number of EC clone cells, and the data was included in the revised Figure 3—figure supplement.

> *(5) Figure 5: The intensity of MTGreen in CH1603 clones seems comparable to that in control cells, at least visually. Since the authors claim a reduction in mitochondrial volume in CG1603 mutants, it is crucial to estimate mitochondrial volume based on MTGreen intensity in mutant and control cells.*

There are two types of clones shown in Figure 5: germ cell clones including all 16 germ cells in the same egg chamber and follicle cell clones. We highlight these two types of clones in the revised Figure 5, to emphasize this point. The total MT Green intensity in both germ cell and follicle cell *CG1603PBac* clones were reduced, compared to germ cells in adjacent egg chambers and adjacent follicle cells in the same egg chamber, respectively. We included the quantification of MTGreen intensity in the revised Figure 5—figure supplement C. Examining mitochondrial number/quantity/size by electron microscopy would further strengthen this statement, and we will consider it in future studies.

> *(6) Figure 8: It would be interesting to know what happens to steady-state mtDNA levels during YL-1 knockdown. If decreased, could overexpressing CG1603 in YL-1 knockdown cells rescue the phenotype?*

YL-1 knockdown reduced steady-state mtDNA levels in eyes, and overexpressing CG1603 restored mtDNA level in YL-1 knockdown cells. These results are included in the revised *Figure 8-figure supplement C*.

> *Minor comments:*
>
> *(7) The paper is lucidly written, but there are minor typos in several places. The authors might proofread it to remove these errors.*

We corrected typos and other minor errors in the manuscript.

> *(8) Quantification for Figure 8 - Supplementary needs to be included.*

We performed the quantification, and the result is shown in Figure 8—figure supplement B.

> ***Reviewer #2 (Recommendations For The Authors):***
>
> *(1) In lines 275-276 and Figure 6E, the authors mention that more than 800 nuclear-encoded mitochondrial genes were reduced by >2-folds in CG1603 mutants. One gene related to mitochondrial replication and three genes related to mtDNA transcription were among them. Was TFAM one of these candidates? What were the reduction levels of TFAM mRNA in RNA seq results? Can the author confirm it via RT-PCR?*

In RNAseq analyses, TFAM was differentially expressed with a log2 Fold-Change of " -0.74", corresponding to ~1.6-fold decrease, and hence was not one of these candidates that were down-regulated more than two folds in CG1603 mutant. Per reviewer's suggestion, we carried out RT-PCR and found TFAM was downregulated about 2-fold in CG1603 mutant. We included this result in the revised Figure 6F and listed all differentially expressed genes in Supplementary file 5a.

> *(2) In many places, the authors argued about the role of CG1603 in ETC biogenesis. Also, the RNA-seq data shows that 64 genes related to the ETC complex were reduced by > 2-fold in CG1603 mutant. Therefore, it would be critical to expand a little on this aspect. For example, what are these genes and related to which of the ETC complex? Can the authors show the reduced levels of some of the candidate genes from each complex via RT-PCR?*

We listed all ETC genes that were down-regulated more than two folds in CG1603 mutant in a separate sheet in Supplementary file 5b. We further validated the reduced expression of ETC genes by RT-PCR on three randomly selected candidate genes from each complex. The result is included in the revised Figure 6F.

> *(3) To make their argument solid on the role of CG1603 on ETC biogenesis, it is important to show the assembly/integrity of ETC complexes as well as the functionality/activity of the ETC complexes in CG1603 mutants.*

We purified mitochondria, and assayed assembly/integrity of three ETC complexes (Complex I, II and IV) and their activities, using blue native PAGE analysis and in gel activity analysis, respectively. The amount of these three complexes, and accordingly, their activities were all markedly reduced in CG1603 mutant compared to wt. The result is included as Figure 4—figure supplement A.

> *(4) CG1603 has already been named as cliff. Why do the authors not use this name, or alternatively propose one?*

We thank the reviewer for the note. The CG1603 has not been named as cliff when we were preparing this manuscript.

> *(5) In lines 230-231, based on the TFAM-GFP and SDHA-mNG levels, the authors claim that "these results demonstrate that CG1603 promotes the expression of both nuclear and mtDNA-encoded ETC genes..." The authors may tone down this statement since it sounds overstating. It would be prudent to claim that a subset of genes are regulated by CG1603.*

We appreciate the reviewer's suggestion. We revised the text to tone down this statement (page 8, line 201; page 9, line 229-230).

https://doi.org/10.7554/eLife.96536.2.sa0